J. Fluid Mech. (2000), *vol.* 405, *pp.* 181–210. Printed in the United Kingdom

© 2000 Cambridge University Press

A fully nonlinear Boussinesq model for surface waves. Part 2. Extension to $O(kh)^4$

By MAURÍCIO F. GOBBI[1], JAMES T. KIRBY[2]† AND GE WEI[3]

[1] Simepar, Caixa Postal 318,80001-970 Curitiba PR, Brasil
[2] Center for Applied Coastal Research, University of Delaware, Newark, DE 19716, USA
[3] CMS Consulting, Suite 219, 6797 North High Street, Worthington, OH 43085, USA

(Received 10 July 1998 and in revised form 30 September 1999)

A Boussinesq-type model is derived which is accurate to $O(kh)^4$ and which retains the full representation of the fluid kinematics in nonlinear surface boundary condition terms, by not assuming weak nonlinearity. The model is derived for a horizontal bottom, and is based explicitly on a fourth-order polynomial representation of the vertical dependence of the velocity potential. In order to achieve a (4,4) Padé representation of the dispersion relationship, a new dependent variable is defined as a weighted average of the velocity potential at two distinct water depths. The representation of internal kinematics is greatly improved over existing $O(kh)^2$ approximations, especially in the intermediate to deep water range. The model equations are first examined for their ability to represent weakly nonlinear wave evolution in intermediate depth. Using a Stokes-like expansion in powers of wave amplitude over water depth, we examine the bound second harmonics in a random sea as well as nonlinear dispersion and stability effects in the nonlinear Schrödinger equation for a narrow-banded sea state. We then examine numerical properties of solitary wave solutions in shallow water, and compare model performance to the full solution of Tanaka (1986) as well as the level 1, 2 and 3 solutions of Shields & Webster (1988).

1. Introduction

Important progress has been made in variable-depth Boussinesq-type models since the development of the more-or-less standard model of Peregrine (1967), which represents a consistent representation of an arbitrary irregular sea state correct to first order in relative wave amplitude $\delta = a/h$ and second order in inverse relative wavelength $\mu = kh$, with $O(\delta) = O(\mu^2) \ll 1$. Madsen, Murray & Sørensen (1991) and Madsen & Sørensen (1992) introduced a rearrangement of dispersive terms in the model equations in order to improve linear dispersion properties. By redefining the dependent variable, Nwogu (1993) achieved the same improvement. Schäffer & Madsen (1995*b*) generalized Nwogu's idea of redefining the dependent variable in Boussinesq models. Wei *et al.* (1995) used Nwogu's approach to derive a Boussinesq-type model (referred to henceforth as the WKGS model) without the weak nonlinearity restriction. Various authors (see, for example, Chen *et al.* 1999 and Madsen, Sørensen & Schäffer 1997) have demonstrated the utility of various $O(\mu^2)$ approximations in the prediction of nearshore wave transformation, surfzone wavebreaking and runup, and the modelling of wave-induced circulation.

† Author to whom correspondence should be addressed: email kirby@udel.edu

https://doi.org/10.1017/S0022112099007247 Published online by Cambridge University Press

Numerical computations indicate that $O(\mu^2)$ models compare very well with solutions of the full potential problem over the range of relevant coastal water depths, except for some discrepancies in the velocity profiles in nearly-breaking waves. These inaccuracies in the prediction of vertical profiles in existing Boussinesq-type models are due to the fact that they assume the velocity profiles to be second-order polynomials in the vertical coordinate z. Dingemans (1973) was the first to introduce $O(\mu^4)$ terms into Boussinesq equations. Other authors, employing rearrangements of terms in models based on quadratic-over-depth flow kinematics, have achieved a (4,4) Padé dispersion relationship in Boussinesq-type models. Those include Madsen *et al.* (1996), Schäffer & Madsen (1995*a*, *b*), and Schröter, Mayerle & Zielke (1994).

In this paper, we derive a fourth-order Boussinesq model in which the velocity potential is approximated by a fourth-order polynomial in z. The model here is derived for a horizontal bottom; an extension to variable depth, an accompanying numerical scheme and various tests against laboratory data are detailed separately in Gobbi & Kirby (1999). A new dependent variable is defined as the weighted average of the velocity potential at two different elevations in the water column, and the weight and positions are chosen to give the very accurate (4,4) Padé approximant of the exact linear dispersion relationship as observed by Witting (1984). The resulting model is first tested for its apparent ability to correctly represent weakly nonlinear wave properties in intermediate water depth. This problem is pursued using a Stokes expansion in powers of δ for arbitrary values of μ. Results at second and third order are examined in comparison to results from the Stokes solution for the full boundary value problem. We then examine numerical solutions of the present model and the WKGS model for the case of solitary waves on water of uniform depth. Results are compared to the full solution of Tanaka (1986) as well as to the first three levels of the Green & Naghdi type formulation of Shields & Webster (1988), denoted here by GN1, GN2 and GN3.

2. Derivation of the $O(\mu^4)$ model

The full boundary value problem for potential flow is given in terms of non-dimensional variables by

$$\phi_{zz} + \mu^2\nabla^2\phi = 0, \qquad -h \leqslant z \leqslant \delta\eta, \tag{1}$$

$$\phi_z + \mu^2\nabla h \cdot \nabla\phi = 0, \qquad z = -h, \tag{2}$$

$$\eta + \phi_t + \tfrac{1}{2}\delta\left[(\nabla\phi)^2 + \frac{1}{\mu^2}(\phi_z)^2\right] = 0, \qquad z = \delta\eta, \tag{3}$$

$$\eta_t + \delta\nabla\phi \cdot \nabla\eta - \frac{1}{\mu^2}\phi_z = 0, \qquad z = \delta\eta. \tag{4}$$

Here, x and y are the horizontal coordinates scaled by a representative wavenumber $k_0 = 2\pi/L_0$, z is the vertical coordinate starting at the still water level and pointing upwards and h is the water depth, both scaled by a typical depth h_0. η is the water surface displacement scaled by a representative amplitude a. ∇ denotes a gradient in horizontal coordinates (x, y). Two dimensionless parameters are apparent: $\delta = a/h_0$ and $\mu^2 = (k_0h_0)^2$. Time t is scaled by $(k_0(gh_0)^{1/2})^{-1}$, and ϕ, the velocity potential, is scaled by $\delta h_0(gh_0)^{1/2}$. We integrate (1) over the water column and use (2) and (4) to

https://doi.org/10.1017/S0022112099007247 Published online by Cambridge University Press

obtain a mass conservation equation

$$\eta_t + \nabla \cdot \boldsymbol{M} = 0, \qquad \boldsymbol{M} \equiv \int_{-h}^{\delta\eta} \nabla\phi \, \mathrm{d}z. \tag{5}$$

We restrict our attention here to a derivation of model equations for waves over a flat bottom of depth h_0; a corresponding variable-depth version of the model has been derived and applied to various examples by Gobbi & Kirby (1999). We assume a fourth-order polynomial approximation for ϕ and choose the coefficients to satisfy the bottom boundary condition (2) (with $\nabla h = 0$) and Laplace's equation (1), retaining terms up $O(\mu^4)$. The approximate potential is given by Mei (1989) as

$$\phi = \phi_0 - \frac{\mu^2(1+z)^2}{2}\nabla^2\phi_0 + \frac{\mu^4(1+z)^4}{24}\nabla^2\nabla^2\phi_0 + O(\mu^6), \tag{6}$$

where ϕ_0 is the velocity potential at the bottom. Commensurate with the extension of the velocity potential to $O(\mu^4)$, we seek to derive a set of model equations having a corresponding dispersion relation in the form of a (4,4) Padé approximant, given by

$$\frac{\tanh\mu}{\mu} = \frac{1 + (1/9)\mu^2 + (1/945)\mu^4}{1 + (4/9)\mu^2 + (1/63)\mu^4} + O(\mu^{10}). \tag{7}$$

For the case of approximations retaining terms to $O(\mu^2)$, the goal of obtaining the corresponding (2,2) Padé approximant may be achieved by redefining the velocity potential in terms of the value of the potential at a normalized elevation $z_\alpha = [(1+2\alpha)^{1/2} - 1]; \alpha = -\frac{2}{5}$ and using the resulting reference value ϕ_α as the dependent variable; see Nwogu (1993), Chen & Liu (1995) or Kirby (1997). Nwogu further introduced a least-squares procedure aimed at minimizing errors in predicted phase speed over a range of μ-values, giving a value of $\alpha = -0.39$ instead of the Padé result. Nwogu's least-square result is used as the basis for determination of the $O(\mu^2)$ results shown subsequently.

The procedure of Nwogu is not adequate for obtaining the (4,4) Padé dispersion relation at $O(\mu^4)$ which we desire here, as discussed by Dingemans (1997) and illustrated in Appendix A. Instead, we define a new dependent variable

$$\tilde{\phi} \equiv \beta\phi_a + (1-\beta)\phi_b, \tag{8}$$

where ϕ_a and ϕ_b are the velocity potentials at elevations $z = z_a$ and $z = z_b$, and β is a weighting parameter. $\tilde{\phi}$ may be written in terms of ϕ_0 using (6) to obtain

$$\tilde{\phi} = \phi_0 - \tfrac{1}{2}\mu^2 B\nabla^2\phi_0 + \tfrac{1}{24}\mu^4 D\nabla^2\nabla^2\phi_0 + O(\mu^6), \tag{9}$$

where

$$B \equiv \beta(1+z_a)^2 + (1-\beta)(1+z_b)^2, \tag{10}$$

$$D \equiv \beta(1+z_a)^4 + (1-\beta)(1+z_b)^4. \tag{11}$$

Inverting (9) gives a formula for ϕ_0 in terms of $\tilde{\phi}$, which in turn is substituted into (6) to get an approximation to the full velocity potential in terms of $\tilde{\phi}$,

$$\phi = \tilde{\phi} + \tfrac{1}{2}\mu^2\left\{B - (1+z)^2\right\}\nabla^2\tilde{\phi} + \tfrac{1}{4}\mu^4\left\{B^2 - B(1+z)^2 - \tfrac{1}{6}D + \tfrac{1}{6}(1+z)^4\right\}\nabla^2\nabla^2\tilde{\phi} + O(\mu^6). \tag{12}$$

Defining the total depth $H = 1 + \delta\eta$, and substituting (12) into (5) gives a mass flux

https://doi.org/10.1017/S0022112099007247 Published online by Cambridge University Press

conservation equation for $\tilde{\phi}$ and η,

$$\eta_t + \nabla \cdot \{H \left[\nabla\tilde{\phi} + \tfrac{1}{2}\mu^2(B - \tfrac{1}{3}H^2)\nabla(\nabla^2\tilde{\phi}) + \tfrac{1}{4}\mu^4(B^2 - B\tfrac{1}{3}H^2 - \tfrac{1}{6}D + \tfrac{1}{30}H^4)\nabla(\nabla^2\nabla^2\tilde{\phi})\right]\} = O(\mu^6). \quad (13)$$

Next we substitute (12) into (3) to obtain an approximate Bernoulli equation,

$$\begin{aligned}\eta &+ \tilde{\phi}_t + \tfrac{1}{2}\mu^2\{B - H^2\}\nabla^2\tilde{\phi}_t \\ &+ \tfrac{1}{4}\mu^4\{B^2 - BH^2 - \tfrac{1}{6}D + \tfrac{1}{6}H^4\}\nabla^2\nabla^2\tilde{\phi}_t \\ &+ \tfrac{1}{2}\delta\left[(\nabla\tilde{\phi})^2 + \mu^2\{B - H^2\}\nabla\tilde{\phi}\cdot\nabla(\nabla^2\tilde{\phi}) + \mu^2H^2(\nabla^2\tilde{\phi})^2\right. \\ &+ \tfrac{1}{2}\mu^4\{B^2 - BH^2 - \tfrac{1}{6}D + \tfrac{1}{6}H^4\}\nabla\tilde{\phi}\cdot\nabla(\nabla^2\nabla^2\tilde{\phi}) \\ &+ \tfrac{1}{4}\mu^4\{B^2 - 2BH^2 + H^4\}\{\nabla(\nabla^2\tilde{\phi})\}^2 \\ &+ \left.\mu^4\{BH^2 - \tfrac{1}{3}H^4\}(\nabla^2\tilde{\phi})(\nabla^2\nabla^2\tilde{\phi})\right] = O(\mu^6). \quad (14)\end{aligned}$$

The model (13) and (14) is referred to subsequently as FN4, for fully-nonlinear fourth order. If we neglect $O(\mu^4)$ terms from (13) and (14) and set $\beta = 1$, we recover the WKGS model with α being related to B by

$$B = 2\alpha + 1. \quad (15)$$

If, in addition, we neglect terms of $O(\delta\mu^2)$ or higher, we recover Nwogu's model in the velocity potential form given by Chen & Liu (1995).

A higher-order model in the standard Boussinesq approximation may be obtained by assuming $\delta/\mu^2 = O(1)$ and retaining terms of $O(\delta\mu^2, \mu^4)$ to obtain the Boussinesq model

$$\eta_t + \nabla \cdot \{\left[H\nabla\tilde{\phi} + \tfrac{1}{2}\mu^2(BH - \tfrac{1}{3}(1 + 3\delta\eta))\nabla(\nabla^2\tilde{\phi}) + \tfrac{1}{4}\mu^4(B^2 - \tfrac{1}{3}B - \tfrac{1}{6}D + \tfrac{1}{30})\nabla(\nabla^2\nabla^2\tilde{\phi})\right]\} = O(\mu^6), \quad (16)$$

$$\eta + \tilde{\phi}_t + \tfrac{1}{2}\mu^2[B - (1 + \delta\eta)]\nabla^2\tilde{\phi}_t + \tfrac{1}{4}\mu^4(B^2 - B - \tfrac{1}{6}D + \tfrac{1}{6})\nabla^2\nabla^2\tilde{\phi}_t + \tfrac{1}{2}\delta\left[(\nabla\tilde{\phi})^2 + \mu^2(B - 1)\nabla\tilde{\phi}\cdot\nabla(\nabla^2\tilde{\phi}) + \mu^2(\nabla^2\tilde{\phi})^2\right] = O(\mu^6, \delta\mu^4). \quad (17)$$

3. Linear model properties

The correct representation of linearized behaviour is a crucial part of ensuring that extended Boussinesq models can be used in relatively deep water. Previous model extensions to the level of (2,2) Padé approximants have allowed models to accurately predict propagation speeds over essentially the entire range of intermediate water depths. However, as will be apparent below, the same models cannot be construed to be accurate predictors of fluid kinematics over the same range of depths, as the quadratic vertical profile associated with standard Boussinesq models is too restrictive to represent the kinematics correctly for μ values of $O(1)$. More recent extensions of these same formulations (Schäffer & Madsen 1995*a*) to (4,4) Padé dispersion extend the propagation range but do nothing to alleviate the restrictions in kinematic prediction associated with the quadratic profile, since the model variables are never related to an assumed form of the potential which retains terms to $O(\mu^4)$.

https://doi.org/10.1017/S0022112099007247 Published online by Cambridge University Press

In contrast, the present model is based initially on a potential which retains this level of information, and the coefficients of that potential may be determined from the spatial structure of the model solution.

In this section, we investigate the properties of the linearization of the model derived in § 2. The accuracy of the (4,4) Padé approximant is demonstrated and, more importantly, we demonstrate the level of correction in kinematic predictions achieved by moving to a fourth-order polynomial dependence in z.

3.1. *Linear dispersion properties*

Neglecting all terms containing δ in (13) and (14) gives a linear mass conservation equation

$$\eta_t + \nabla^2\tilde{\phi} - \mu^2 C_1 \nabla^2\nabla^2\tilde{\phi} + \mu^4 C_2 \nabla^2\nabla^2\nabla^2\tilde{\phi} = 0, \tag{18}$$

and Bernoulli equation

$$\eta + \tilde{\phi}_t - \mu^2 C_3 \nabla^2\tilde{\phi}_t + \mu^4 C_4 \nabla^2\nabla^2\tilde{\phi}_t = 0, \tag{19}$$

where

$$C_1 \equiv -\tfrac{1}{2}(B - \tfrac{1}{3}), \tag{20}$$

$$C_2 \equiv \tfrac{1}{4}(B^2 - \tfrac{1}{3}B - \tfrac{1}{6}D + \tfrac{1}{30}), \tag{21}$$

$$C_3 \equiv -\tfrac{1}{2}(B - 1), \tag{22}$$

$$C_4 \equiv \tfrac{1}{4}(B^2 - B - \tfrac{1}{6}D + \tfrac{1}{6}). \tag{23}$$

In order to analyse the dispersion properties of these equations, we assume the following general solution:

$$\eta = a\mathrm{e}^{\mathrm{i}(\boldsymbol{x}-\omega t)}, \qquad \tilde{\phi} = b\mathrm{e}^{\mathrm{i}(\boldsymbol{x}-\omega t)}, \tag{24}$$

where ω is the angular frequency non-dimensionalized by $k_0(gh_0)^{1/2}$, a and b are amplitudes, and $\mathrm{i} = \sqrt{-1}$. Substituting (24) into (18) and (19) we obtain the linear dispersion relationship for the model,

$$\omega^2 = \frac{1 + C_1\mu^2 + C_2\mu^4}{1 + C_3\mu^2 + C_4\mu^4}. \tag{25}$$

Choosing $C_1 - C_4$ to force (25) to correspond to the (4,4) Padé approximant (7) gives $B = 1/9$ and $D = 5/189$. We then solve for parameters β, z_a, and z_b. Since we have three unknowns but only two equations defining B and D, there is an infinite number of solutions that give the desired values of B and D. However, an arbitrary choice of β can give imaginary values of z_a or z_b or values lying outside the fluid domain, causing the related potential values to lose physical significance. The relationship between β, z_a, and z_b is given by

$$z_a = \left[\frac{1}{9} - \left\{\frac{8\beta}{567(1-\beta)}\right\}^{1/2} + \left\{\frac{8}{567\beta(1-\beta)}\right\}^{1/2}\right]^{1/2} - 1, \tag{26}$$

$$z_b = \left[\frac{1}{9} - \left\{\frac{8\beta}{567(1-\beta)}\right\}^{1/2}\right]^{1/2} - 1. \tag{27}$$

Figure 1 shows a plot of the real part of z_a and z_b as given by (27). A choice of values of β between 0.018 and 0.467 will cause both z_a and z_b to be real values lying

https://doi.org/10.1017/S0022112099007247 Published online by Cambridge University Press

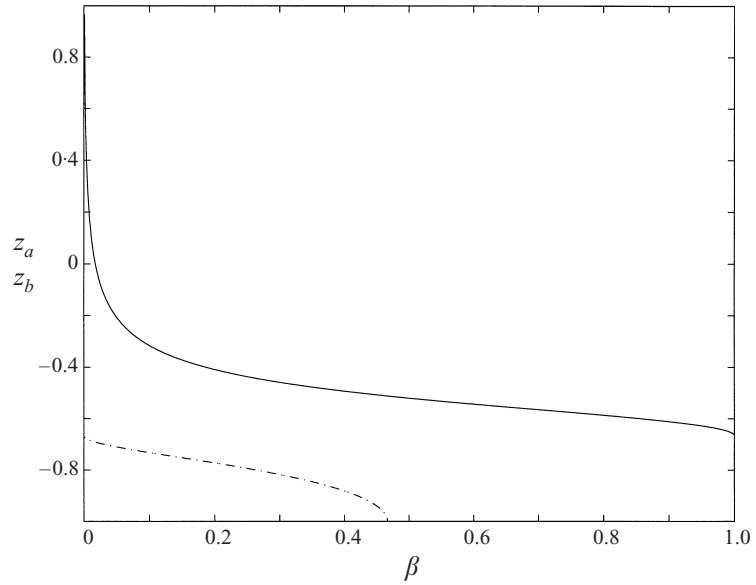


FIGURE 1. Values of $z_a(\beta)$ (solid), $z_b(\beta)$ (dash–dot) as a function of weighting factor β, corresponding to the (4,4) Padé approximant dispersion relation.

inside the water column. For the case of constant water depth, the model coefficients are fixed by the choice of B and D and thus the further choice of β has no influence on the model equations. For the case of variable depth the value of β could be used to optimize depth-dependent properties such as linear shoaling. However, actual wave calculations showed that even the variable-depth version of the model (Gobbi, Kennedy & Kirby 1998) was not very sensitive to choices of the parameter β.

Figure 2 shows a comparison of the ratio of the model phase speed to Airy's exact linear solution for the standard $O(\mu^2)$ Boussinesq theory based on depth-averaged velocity (with normalized phase speed C given by $C^2 = (1 + \mu^2/3)^{-1}$, Nwogu's least-square formulation based on velocity at z_α, and the present model with a (4,4) Padé dispersion relationship. It is clear that the present model has improved linear dispersion properties over Nwogu's model and closely reproduces the exact solution through intermediate to deep water. Similarly, the linear group velocity, defined as $C_g = \partial\omega/\partial k$, is shown in figure 3, and the improvement over Nwogu's result is even more evident.

As an alternative procedure to choosing the (4,4) Padé approximant as a basis for determining the dispersion relation, one could compute values for β, z_a, and z_b to minimize the errors in the linear phase speed and group velocity over some depth range. This was the procedure used by Nwogu to obtain his optimized parameter $\alpha = -0.39$. However, the authors found that the dispersion relation error surface in the neighbourhood of coefficient values corresponding to the (4,4) Padé approximant is extremely flat, and any parameter optimization over a normal water depth range would result in minor improvement in overall model properties.

3.2. *Internal kinematics*

The internal kinematics of the present model can be obtained from (12) and (24). Note that $O(\mu^2)$ model results can be obtained from the present model as explained at the end of § 2. Based on periodic solutions of the form (24), we define a function

https://doi.org/10.1017/S0022112099007247 Published online by Cambridge University Press

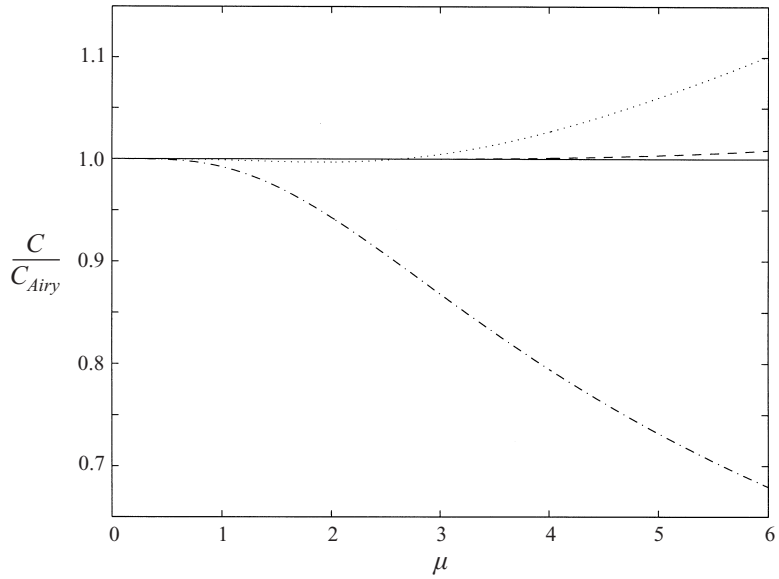


FIGURE 2. Ratio of model linear phase speed to Airy's exact linear solution. Standard Boussinesq (dash–dot), Nwogu, $\alpha = -0.39$ (dot), present (4,4) Padé (dash).

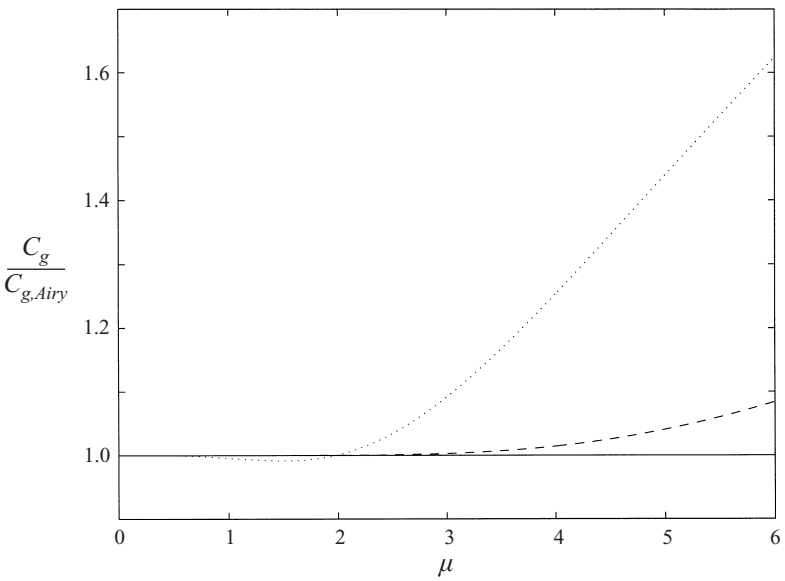


FIGURE 3. Ratio of model linear group velocity to Airy's exact linear solution. Nwogu, $\alpha = -0.39$ (dot), present (4,4) Padé (dash).

$f_1(z)$ as the the velocity potential (or any horizontal velocity component) normalized by its value at position $z = 0$:

$$f_1(z) = \frac{1 - \frac{1}{2}\mu^2[B - (1+z)^2] + \frac{1}{4}\mu^4[B^2 - B(1+z)^2 - \frac{1}{6}D + \frac{1}{6}(1+z)^4]}{1 - \frac{1}{2}\mu^2[B - 1] + \frac{1}{4}\mu^4[B^2 - B - \frac{1}{6}D + \frac{1}{6}]}. \tag{28}$$

The vertical velocity component w can be obtained by differentiating (12) with respect to z. Similarly to f_1, a vertical velocity profile function can be obtained by

https://doi.org/10.1017/S0022112099007247 Published online by Cambridge University Press

defining $f_2(z) = w(z)/w(0)$:

$$f_2(z) = \frac{\mu^2[(1+z)] + \frac{1}{2}\mu^4[-B(1+z) + \frac{1}{3}(1+z)^3]}{\mu^2 + \frac{1}{2}\mu^4[-B + \frac{1}{3}]}. \tag{29}$$

Figure 4 shows comparisons of $f_1(z)$ between the exact linear solution $f_1(z) = \cosh[\mu(1+z)]/\cosh[\mu]$, the $O(\mu^2)$ model and the present $O(\mu^4)$ model for various values of relative water depth μ. Notice that for moderately shallow water, the two models reproduce the exact solution quite well. As μ increases, the velocity profile predicted by $O(\mu^2)$ models (exemplified here by the Nwogu-type model) start to deviate strongly from the exact solution, developing a flow reversal near the bottom at $\mu = \sqrt{10} \approx 3.16$. The present model remains very accurate over this range of depths. In deeper water (indeed, well beyond a nominal deep-water limit of $\mu = \pi$), the present model starts to deviate from the exact solution. First, an inflection point develops at the bottom at $\mu^2 = 18$ ($\mu \approx 4.24$). For higher values of μ, the inflection point moves up in the water column. At the same time, a vertical tangent at an elevation higher than the inflection point occurs. The first flow reversal occurs at the point where the value of f_1 at the vertical tangent falls to zero. This is at $\mu^2 = 18 + 9\sqrt{2}$ ($\mu \approx 5.54$) at an elevation given by $(1+z)^2 = \sqrt{2}/(6+3\sqrt{2})$, or $z \approx -0.628$.

The exact linear solution for $f_2(z)$, which describes the vertical profile of vertical velocity, is given by $f_2(z) = \mu\sinh[\mu(1+z)]/\cosh[\mu]$. Figure 5 shows results similar to figure 4 for $f_2(z)$. All $O(\mu^2)$ models have a linear vertical profile for w, which is a poor representation of the solution in intermediate to deep water. The present model stays close to the exact solution for a wide range of μ. A reversal of the vertical flow starts to appear at the inflection point in the horizontal velocity profile, given by $(1+z)^2 = (1 - 18/\mu^2)/9$, and occurs first at $\mu \approx 4.24$, as indicated above.

Finally, we consider the aspect ratio $f_3(\mu) = w/u$ of the wave orbital motion at $z = 0$, as predicted by the model. Figure 6 shows the ratio of model f_3 to the exact linear solution $f_3(\mu) = \tanh(\mu)$ for the present $O(\mu^4)$ model and for the $O(\mu^2)$ model. The approximate expression for f_3 is given by

$$f_3(\mu) = \frac{w(z=0)}{u(z=0)} = \frac{\mu + \frac{1}{2}\mu^3[-B + \frac{1}{3}]}{1 - \frac{1}{2}\mu^2[B-1] + \frac{1}{4}\mu^4[B^2 - B - \frac{1}{6}D + \frac{1}{6}]}. \tag{30}$$

Again, the present model predicts the aspect ratio better than the $O(\mu^2)$ model, and with reasonable accuracy over the range $0 \leqslant \mu \leqslant 3$.

4. Nonlinear properties in intermediate water depth

In the previous sections we have seen that the proposed model has excellent linear dispersion properties as well as greatly improved representation of the internal flow kinematics. It is useful to analyse some of the nonlinear properties of the model by using analytical tools such as Stokes-type asymptotic expansions and multiple scales expansions. Since these types of analysis have been extensively applied and studied for the full boundary value problem for the velocity potential, we can obtain an idea of how well the nonlinear version of the present model would perform in intermediate water depth by comparing some of its nonlinear properties with those of the full problem and also with the WKGS and Nwogu models. In the following subsections we investigate $O(\delta)$ nonlinear interactions in a random sea, and $O(\delta^2)$ evolution of a narrow-banded wave train governed by the cubic Schrödinger equation.

https://doi.org/10.1017/S0022112099007247 Published online by Cambridge University Press

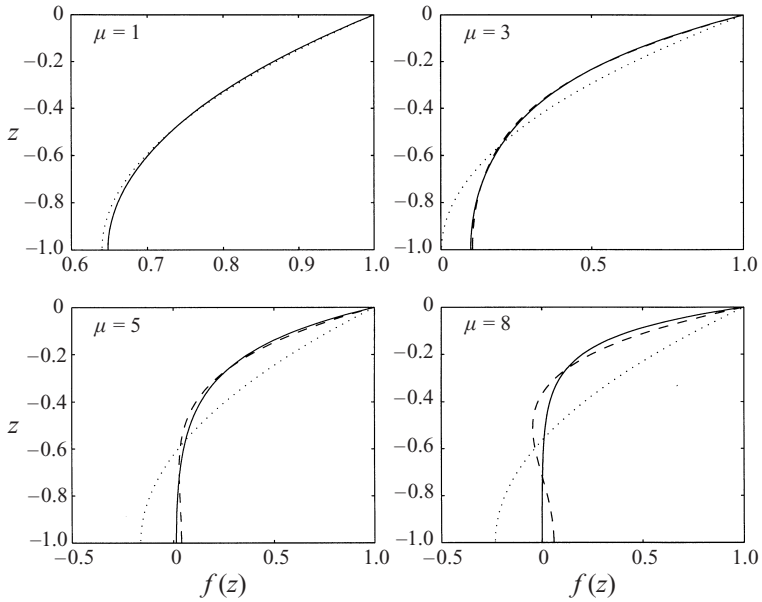


FIGURE 4. Normalized vertical profile of linear horizontal velocity for four values of μ. Exact linear solution (solid), $O(\mu^2)$ approximate solution (dot), present $O(\mu^4)$ approximate solution (dash).

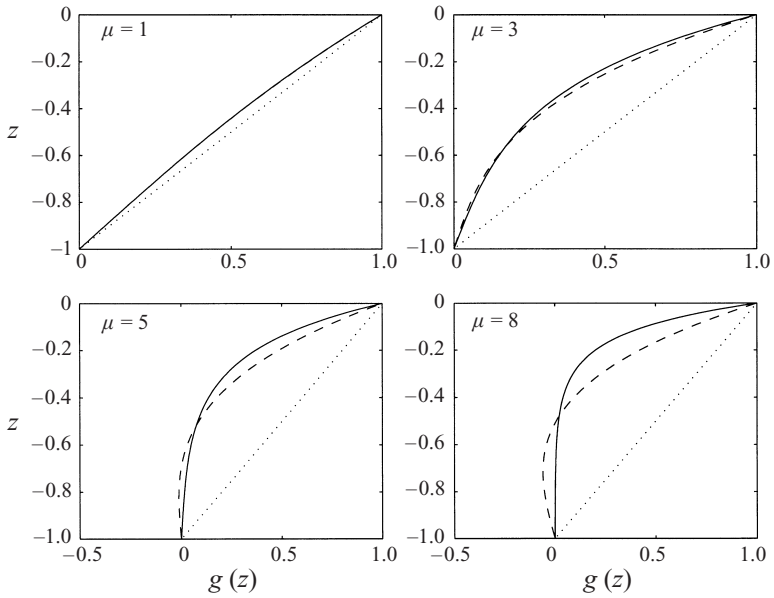


FIGURE 5. Normalized vertical profile of linear vertical velocity for four values of μ. Exact linear solution (solid), $O(\mu^2)$ approximate solution (dot), present $O(\mu^4)$ approximate solution (dash).

4.1. *Second-order random sea*

We first examine the generation of super- and subharmonics by second-order Stokes-type interactions. It is well known that in intermediate and deep water the first nonlinear correction of a linear wave solution is a set of bound waves, also called superharmonics (resulting from sum-wave interactions) and subharmonics (resulting

https://doi.org/10.1017/S0022112099007247 Published online by Cambridge University Press

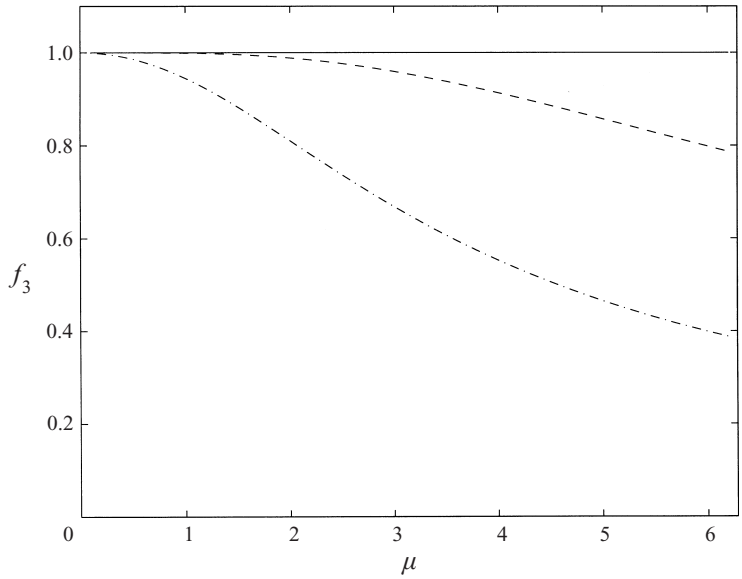


FIGURE 6. Ratio of approximate values for the aspect ratio $f_3 = w(0)/u(0)$ to the exact linear solution. $O(\mu^2)$ approximate solution (dash–dot), present $O(\mu^4)$ approximate solution (dash).

from difference-wave interactions) (Hasselmann 1962). These bound waves are proportional to products of the amplitudes of solutions to the linear equations. The constants of proportionality, which are functions of the local depth, will be referred to as transfer coefficients. Nwogu (1993) has investigated the generation of these bound waves in his extended Boussinesq model and found qualitatively reasonable agreement with Stokes' theory. Madsen & Sørensen (1993) have found similar results. Kirby & Wei (1994) extended Nwogu's model to a fully nonlinear formulation and found that the retention of terms proportional to $\delta\mu^2$ (which are neglected in Nwogu's model and the standard Boussinesq model by assumption) is essential to a prediction of the transfer coefficients, which is to the order of retained dispersive terms in the original model equations. Here, we derive the transfer coefficients for the present model and compare to results from previous models.

We proceed by introducing the perturbation expansion

$$\eta = \eta_0 + \delta\eta_1 + \delta^2\eta_2 + \cdots, \tag{31}$$

$$\tilde{\phi} = \phi_0 + \delta\phi_1 + \delta^2\phi_2 + \cdots, \tag{32}$$

into (13) and (14), and ordering the equations by powers of δ. At each order $O(\delta^n)$ we obtain

$$\eta_{nt} + \mathrm{L}_1\phi_n = F_n, \tag{33}$$

$$\eta_n + \mathrm{L}_2\phi_{nt} = G_n, \tag{34}$$

where L_1 and L_2 are the linear operators

$$\mathrm{L}_1 \equiv \nabla^2 + \tfrac{1}{2}\mu^2(B - \tfrac{1}{3})\nabla^2\nabla^2 + \tfrac{1}{4}\mu^4(B^2 - \tfrac{1}{3}B - \tfrac{1}{6}D + \tfrac{1}{30})\nabla^2\nabla^2\nabla^2, \tag{35}$$

$$\mathrm{L}_2 \equiv 1 + \tfrac{1}{2}\mu^2(B - 1)\nabla^2 + \tfrac{1}{4}\mu^4(B^2 - B - \tfrac{1}{6}D + \tfrac{1}{6})\nabla^2\nabla^2, \tag{36}$$

and the forcing terms for $n = 0$, 1, and 2 are given by

$$F_0 \equiv 0, \tag{37}$$

https://doi.org/10.1017/S0022112099007247 Published online by Cambridge University Press

$$G_0 \equiv 0, \tag{38}$$

$$F_1 \equiv -\nabla\cdot(\eta_0\nabla\phi_0) - \tfrac{1}{2}\mu^2(B-1)\nabla\cdot\{\eta_0\nabla(\nabla^2\phi_0)\} - \tfrac{1}{4}\mu^4(B^2-B-\tfrac{1}{6}D+\tfrac{1}{6})\nabla\cdot\{\eta_0\nabla(\nabla^2\nabla^2\phi_0)\}, \tag{39}$$

$$\begin{aligned} G_1 \equiv {} & -\tfrac{1}{2}(\nabla\phi_0)^2 + \tfrac{1}{2}\mu^2\{2\eta_0\nabla^2\phi_{0_t} - (B-1)\nabla\phi_0\cdot\nabla(\nabla^2\phi_0) + (\nabla^2\phi_0)^2\} \\ & -\tfrac{1}{4}\mu^4\{(\tfrac{2}{3}-2B)\eta_0\nabla^2\nabla^2\phi_{0_t} + (B^2-B-\tfrac{1}{6}D+\tfrac{1}{6})\nabla\phi_0\cdot\nabla(\nabla^2\nabla^2\phi_0) \\ & +\tfrac{1}{2}(B-1)^2\nabla(\nabla^2\phi_0)\cdot\nabla(\nabla^2\phi_0) + 2(B-\tfrac{1}{3})(\nabla^2\phi_0)(\nabla^2\nabla^2\phi_0)\}, \end{aligned} \tag{40}$$

$$\begin{aligned} F_2 \equiv {} & -\nabla\cdot(\eta_1\nabla\phi_0) - \nabla\cdot(\eta_0\nabla\phi_1) \\ & -\tfrac{1}{2}\mu^2\left[(B-1)[\nabla\cdot\{\eta_1\nabla(\nabla^2\phi_0)\} + \nabla\cdot\{\eta_0\nabla(\nabla^2\phi_1)\}] - \nabla\cdot\{\eta_0^2\nabla(\nabla^2\phi_0)\}\right] \\ & -\tfrac{1}{4}\mu^4\left[(B^2-B-\tfrac{1}{6}D+\tfrac{1}{6})\left[\nabla\cdot\{\eta_1\nabla(\nabla^2\nabla^2\phi_0)\} + \nabla\cdot\{\eta_0\nabla(\nabla^2\nabla^2\phi_1)\}\right]\right. \\ & \left. -(B-\tfrac{1}{3})\nabla^2\cdot\{\eta_0^2\nabla(\nabla^2\nabla^2\phi_0)\}\right], \end{aligned} \tag{41}$$

$$\begin{aligned} G_2 \equiv {} & -\nabla\phi_1\cdot\nabla\phi_0 - \tfrac{1}{2}\mu^2\{-2[\eta_1\nabla^2\phi_{0_t} + \eta_0\nabla^2\phi_{1_t}] \\ & +(B-1)[\nabla\phi_0\cdot\nabla(\nabla^2\phi_1) + \nabla\phi_1\cdot\nabla(\nabla^2\phi_0)] \\ & +2\nabla^2\phi_0\nabla^2\phi_1 - \eta_0^2\nabla^2\phi_{0_t} - 2\eta_0\nabla\phi_0\cdot\nabla(\nabla^2\phi_0) + 2\eta_0(\nabla^2\phi_0)^2\} \\ & -\tfrac{1}{4}\mu^4\{-2(B-\tfrac{1}{3})[\eta_1\nabla^2\nabla^2\phi_{0_t} + \eta_0\nabla^2\nabla^2\phi_{1_t}] \\ & +(B^2-B-\tfrac{1}{6}D+\tfrac{1}{6})[\nabla\phi_1\cdot\nabla(\nabla^2\nabla^2\phi_0) + \nabla\phi_0\cdot\nabla(\nabla^2\nabla^2\phi_1)] \\ & +(B-1)^2\nabla(\nabla^2\phi_1)\cdot\nabla(\nabla^2\phi_0) \\ & +2(B-\tfrac{1}{3})[(\nabla^2\phi_1)(\nabla^2\nabla^2\phi_0) + (\nabla^2\phi_0)(\nabla^2\nabla^2\phi_1)] \\ & -(B-1)\eta_0^2\nabla^2\nabla^2\phi_{0_t} - 2(B-\tfrac{1}{3})\eta_0\nabla\phi_0\cdot\nabla(\nabla^2\nabla^2\phi_0) \\ & -2(B-1)\eta_0\nabla(\nabla^2\phi_0)\cdot\nabla(\nabla^2\phi_0) + 4(B-\tfrac{2}{3})\eta_0(\nabla^2\phi_0)(\nabla^2\nabla^2\phi_0)\}. \end{aligned} \tag{42}$$

We now assume the following random sea as the solution to the $O(1)$ problem:

$$\eta_0 = \sum_n a_n\cos\psi_n, \qquad \phi_0 = \sum_n b_n\sin\psi_n, \tag{43}$$

where a_n and b_n are non-dimensional amplitudes of the functions η_0 and ϕ_0, $\psi_n = \boldsymbol{k}_n\cdot\boldsymbol{x} - \omega_n t$, $\boldsymbol{k}_n$ is the n-component wavenumber vector non-dimensionalized by k_0, $\boldsymbol{x}$ is the horizontal coordinates vector non-dimensionalized by $1/k_0$, ω_n is the n-component angular frequency non-dimensionalized by $k_0(gh_0)^{1/2}$. Substitution of (43) into the $O(1)$ set of equations gives a set of n linear dispersion relationships between ω_n and $k_n = |\boldsymbol{k}_n|$:

$$\omega_n^2 = k_n^2\frac{1-\frac{1}{2}(B-\frac{1}{3})\mu^2k_n^2 + \frac{1}{4}(B^2-\frac{1}{3}B-\frac{1}{6}D+\frac{1}{30})\mu^4k_n^4}{1-\frac{1}{2}(B-1)\mu^2k_n^2 + \frac{1}{4}(B^2-B-\frac{1}{6}D+\frac{1}{6})\mu^4k_n^4}. \tag{44}$$

https://doi.org/10.1017/S0022112099007247 Published online by Cambridge University Press

We also find a relationship between a_n and b_n given by:

$$b_n = \frac{\omega_n}{k_n K_n} a_n, \quad K_n = k_n \left\{1 - \tfrac{1}{2}\mu^2 k_n^2 (B - \tfrac{1}{3}) + \tfrac{1}{4}\mu^4 k_n^4 (B^2 - \tfrac{1}{3}B - \tfrac{1}{6}D + \tfrac{1}{30})\right\}. \tag{45}$$

Following the standard perturbation technique, we substitute the $O(1)$ solution (43) into the right-hand side of the $O(\delta)$ equations (34) to find the forcing of the $O(\delta)$ problem. The forcings F_1 and G_1 in the mass and dynamic equations (34) respectively are

$$F_1 = \frac{1}{4} \sum_l \sum_m a_m a_l \left\{ \mathscr{F}^+_{ml} \sin(\phi_l + \phi_m) + \mathscr{F}^-_{ml} \sin(\phi_l - \phi_m) \right\}, \tag{46}$$

$$G_1 = \frac{1}{4} \sum_l \sum_m a_m a_l \left\{ \mathscr{G}^+_{ml} \cos(\phi_l + \phi_m) + \mathscr{G}^-_{ml} \cos(\phi_l - \phi_m) \right\}, \tag{47}$$

where

$$\mathscr{F}^{\pm}_{ml} = \frac{\omega_m k_l^2 \pm \omega_l k_m^2 + (\omega_l \pm \omega_m)(\boldsymbol{k}_l \cdot \boldsymbol{k}_m)}{\omega_l \omega_m}, \tag{48}$$

$$\begin{aligned} \mathscr{G}^{\pm}_{ml} = \frac{1}{k_l k_m K_l K_m} \big[& - \omega_l \omega_m (\boldsymbol{k}_l \cdot \boldsymbol{k}_m) + \mu^2 \big\{ \omega_m^2 k_m^2 k_l K_l \\ & + \omega_l^2 k_l^2 k_m K_m + \tfrac{1}{2}(B-1)\omega_l \omega_m (k_l^2 + k_m^2)(\boldsymbol{k}_l \cdot \boldsymbol{k}_m) \pm \omega_l \omega_m k_l^2 k_m^2 \big\} \\ & + \mu^4 \big\{ - \tfrac{1}{2}\big(B - \tfrac{1}{3}\big) \left(\omega_l^2 k_l^4 k_m K_m + \omega_m^2 k_m^4 k_l K_l\right) \\ & - \tfrac{1}{4}\big(B^2 - B - \tfrac{1}{6}D + \tfrac{1}{6}\big) (\boldsymbol{k}_l \cdot \boldsymbol{k}_m) \omega_l \omega_m (k_l^4 + k_m^4) \\ & - \tfrac{1}{4}(B-1)^2 \omega_l \omega_m k_l^2 k_m^2 (\boldsymbol{k}_l \cdot \boldsymbol{k}_m) \mp \tfrac{1}{2}\big(B - \tfrac{1}{3}\big) \omega_m \omega_l k_m^2 k_l^2 (k_m^2 + k_l^2) \big\} \big]. \end{aligned} \tag{49}$$

Equation (48) is identical to the full Stokes' theory result, except for the approximation inherent in the (4,4) Padé dispersion relationship. Equation (49) can be rearranged within the level of approximation of the present model to

$$\mathscr{G}^{\pm}_{ml} = \frac{-\boldsymbol{k}_l \cdot \boldsymbol{k}_m + \mu^2 \left\{ \omega_l \omega_m (\omega_l^2 + \omega_m^2) \pm \omega_l^2 \omega_m^2 \right\}}{\omega_l \omega_m} + O(\mu^6), \tag{50}$$

which is, again, formally the same as the full Stokes' theory result but with an approximate dispersion relationship.

The forced solution for η_1 can be obtained by solving (34) and is given by

$$\eta_1 = \sum_l \sum_m a_m a_l \left\{ \mathscr{H}^+_{ml} \cos(\phi_l + \phi_m) + \mathscr{H}^-_{ml} \cos(\phi_l - \phi_m) \right\}, \tag{51}$$

where

$$\mathscr{H}^{\pm}_{ml} = \frac{\omega^{\pm}_{ml} \mathscr{F}^{\pm}_{ml} - k^{\pm}_{ml} \mathscr{G}^{\pm}_{ml} T^{\pm}_{ml}}{4\left[(\omega^{\pm}_{ml})^2 - k^{\pm}_{ml} T^{\pm}_{ml}\right]}, \tag{52}$$

$$T^{\pm}_{ml} \equiv k^{\pm}_{ml} \frac{1 - \frac{1}{2}\mu^2 (B - \frac{1}{3})(k^{\pm}_{ml})^2 + \frac{1}{4}\mu^4 (B^2 - \frac{1}{3}B - \frac{1}{6}D + \frac{1}{30})(k^{\pm}_{ml})^4}{1 - \frac{1}{2}\mu^2 (B-1)(k^{\pm}_{ml})^2 + \frac{1}{4}\mu^4 (B^2 - B - \frac{1}{6}D + \frac{1}{6})(k^{\pm}_{ml})^4}, \tag{53}$$

$$k^{\pm}_{ml} = |\boldsymbol{k}_l \pm \boldsymbol{k}_m|, \qquad \omega^{\pm}_{ml} = \omega_l \pm \omega_m. \tag{54}$$

$\mathscr{H}^+_{ml}$, $\mathscr{H}^-_{ml}$ are respectively the super- and subharmonic transfer coefficients of the

https://doi.org/10.1017/S0022112099007247 Published online by Cambridge University Press

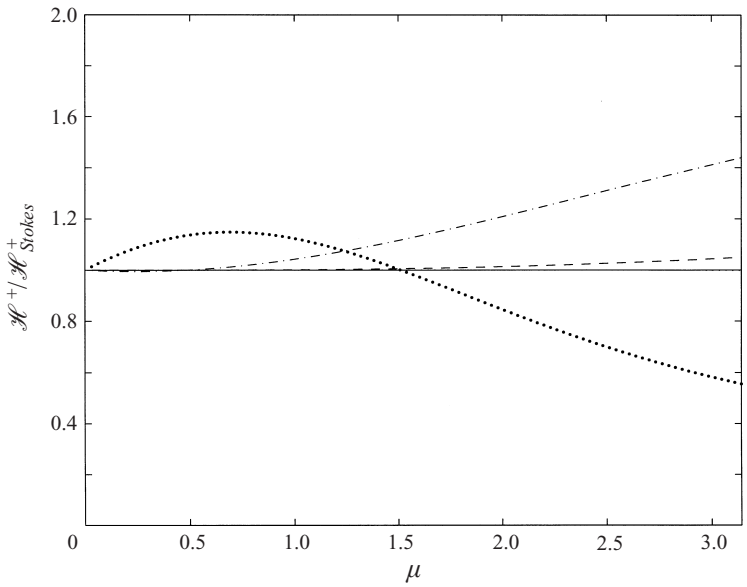


FIGURE 7. Ratio of approximate superharmonic transfer coefficients to Stokes' solution. Self-interaction between two identical waves. Stokes' theory (solid), Nwogu (dot), WKGS (dash–dot), present model (dash).

interaction between the (l, m) pair of waves. Figures 7 and 8 show comparisons of the ratio of $\mathscr{H}^{\pm}_{ml}$ to Stokes' solution, for Nwogu's model, the WKGS model, and the present model, for the self-interaction between two identical waves, with $\omega_m = \omega_l, \boldsymbol{k}_m = \boldsymbol{k}_l$. Note that the poor representation of these coefficients at small μ in Nwogu's model is due to the assumption of weak nonlinearity, as discussed by Kirby & Wei (1994). The present model predicts superharmonic amplitudes very accurately over a wide range of water depths. The asymptotic representation of subharmonic amplitudes is also more accurate than in previous models, but the new solution deviates more rapidly from the exact solution than do the previous results.

4.2. *Third-order nonlinear interactions: Schrödinger equation*

We now extend our analysis to third-order interactions by deriving a cubic Schrödinger equation (which governs the evolution of a wave envelope associated with the propagation of a narrow-banded-spectrum wave train) for the present model and comparing some of its properties with the full boundary value problem, and also with the WKGS fully nonlinear second-order model. The detailed derivation of the equation for the present model will not be shown since it is very similar to the derivation for the full boundary value problem, which can be found in Mei (1989), and can be done using a standard WKB multiple scales approach. We now outline the derivation. A narrow-banded wave train with carrier wavenumber k_0 and angular frequency ω is assumed to be propagating mainly in the x-direction. The time and space variables are split into fast and slow contributions

$$t = t' + \delta t' + \delta^2 t' = t' + T_1 + T_2, \tag{55}$$

$$x = x' + \delta x' + \delta^2 x' = x' + X_1 + X_2, \tag{56}$$

$$y = \delta y' + \delta^2 y' = Y_1 + Y_2. \tag{57}$$

https://doi.org/10.1017/S0022112099007247 Published online by Cambridge University Press

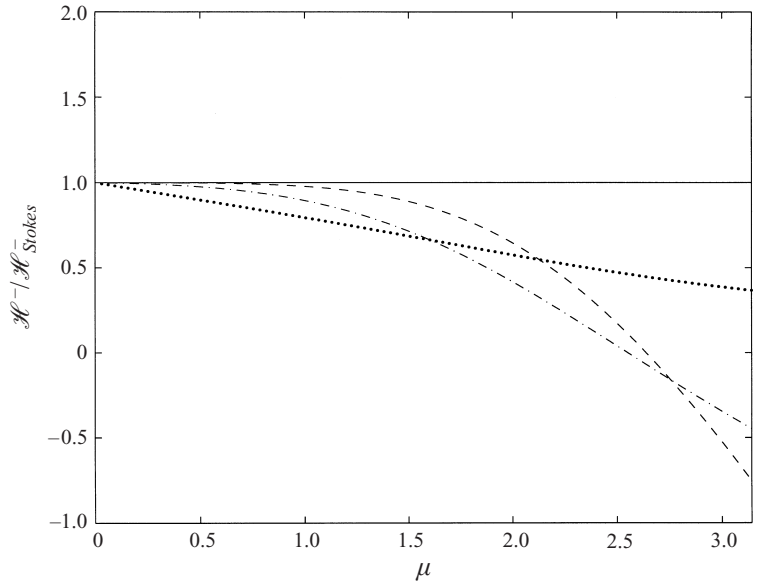


FIGURE 8. Ratio of approximate subharmonic transfer coefficients to Stokes' solution. Self-interaction between two identical waves. Stokes' theory (solid), Nwogu (dot), WKGS (dash–dot), present model (dash).

Notice that y has only slow scale contributions. We expand the dependent variables as

$$\eta = \delta\eta_1 + \delta^2\eta_2 + \delta^3\eta_3, \tag{58}$$

$$\tilde{\phi} = \delta\phi_1 + \delta^2\phi_2 + \delta^3\phi_3. \tag{59}$$

We then substitute (57) and (59) into (13) and (14), and order the equations in a manner analogous to what was done in the previous section. We assume the solution to each order to be of the form

$$\eta_n = \sum_{m=-n}^{n} \eta_{nm}(X_1, X_2, Y_1, Y_2, T_1, T_2)\mathrm{e}^{\mathrm{i}m(x'-\omega t')}, \tag{60}$$

$$\phi_n = \sum_{m=-n}^{n} \phi_{nm}(X_1, X_2, Y_1, Y_2, T_1, T_2)\mathrm{e}^{\mathrm{i}m(x'-\omega t')}. \tag{61}$$

We then seek an equation for the evolution of the wave envelope in X_1 and T_1 by applying solvability conditions at each order. After some algebra, a system of equations governing the wave-induced mean flow and the short-wave envelope is found. The equation for the slowly-varying mean flow is given by

$$-\phi_{10T_1T_1} + (\phi_{10X_1X_1} + \phi_{10Y_1Y_1}) = \frac{\delta}{2\omega\mu}(|A|^2_{X_1} + S_0|A|^2_{T_1}), \tag{62}$$

where

$$S_0 = \frac{-\omega^3[1 - C1\mu^2][1 + (1 + 2C_3)\mu^2 + (2C_4 + C_3^2 + 2C_1)\mu^4]}{2[1 + C_1\mu^2 + C_2\mu^4]}. \tag{63}$$

https://doi.org/10.1017/S0022112099007247 Published online by Cambridge University Press

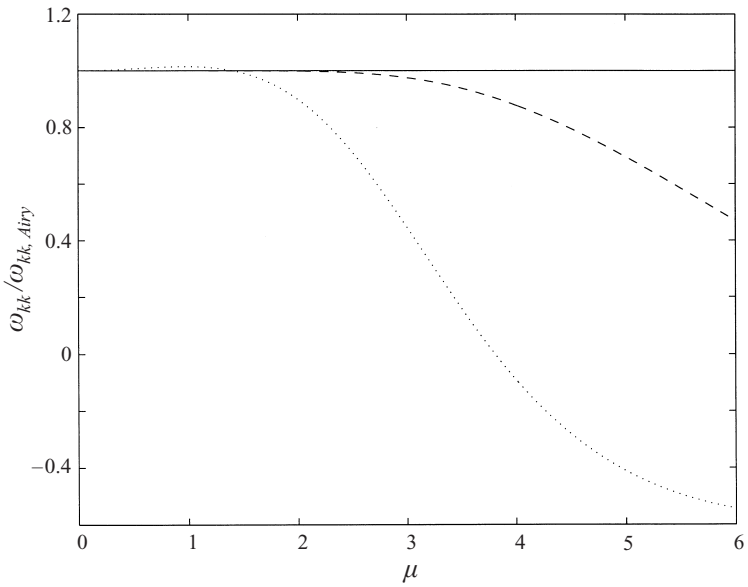


FIGURE 9. Ratio of approximate $\partial^2\omega/\partial k^2$ to exact linear solution result. Nwogu, $\alpha = -0.39$ (dot), present (dash).

The cubic Schrödinger equation for the short-wave envelope is given by

$$A_{T_2} + C_g A_{X_2} - \tfrac{1}{2}\mathrm{i}\omega'' A_{X_1X_1} - \tfrac{1}{2}\mathrm{i}C_g A_{Y_1Y_1} + \mathrm{i}\delta^2\mu^2\sigma_1|A|^2 A + \mathrm{i}\delta\mu\left\{\phi_{10X_1} + \frac{1 + C_3\mu^2 + C_4\mu^4 - \mu^2\omega^2\left(1 + C_1\mu^2\right)}{2\omega\left(1 + C_3\mu^2 + C_4\mu^4\right)}\phi_{10T_1}\right\}A = 0, \qquad (64)$$

where $A = 2\eta_{11}$ is the envelope amplitude, $\omega'' = \partial^2\omega/\partial k^2$ (shown in comparison to the full linear theory result in figure 9), and expressions for C_1, C_3, and C_4 are given above in (20)–(23). The coefficient σ_1 is given in Appendix B for both the present model and the full potential problem. Restricting attention to waves propagating in the x-direction with no transverse variation ($\partial/\partial Y_1 \equiv 0$), a final equation for the case of modulated waves in the presence of a long wave locked to the wave disturbance can be obtained after integration of (62) in a frame moving with the group velocity and substitution in (64), and is given by

$$-\mathrm{i}A_\tau - \tfrac{1}{2}\omega'' A_{\xi\xi} + \delta^2\mu^2\sigma|A|^2 A + \gamma_1(\tau)A = 0, \qquad (65)$$

where $\tau = \delta T_1$, $\xi = X_1 - C_g T_1$, and γ_1 is an arbitrary function of τ. The last term can be absorbed into a new variable by the transformation $A' = A^{\mathrm{i}\int\gamma_1\,\mathrm{d}\tau}$. The coefficient σ (illustrated in figure 10) is the sum of contributions from the wave–wave interactions σ_1 and wave–current interactions σ_2, also given in Appendix B for the present model as well as for the full potential problem.

For the case of an unmodulated wave train, with $\phi_{10} = UX_1 + gbT_1$ (U, b constants), (64) can be used to obtain the frequency shift associated with amplitude dispersion. The equation becomes

$$\frac{\partial A}{\partial T_2} + \mathrm{i}\omega_2|A|^2 A = 0, \qquad (66)$$

https://doi.org/10.1017/S0022112099007247 Published online by Cambridge University Press

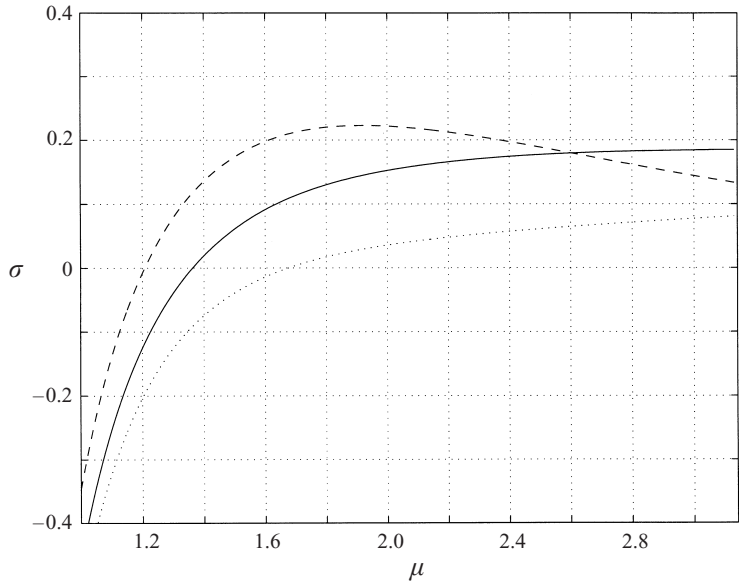


FIGURE 10. Schrödinger equation's cubic term coefficient σ. WKGS (dot), present (dash).

where

$$\omega_2 = \sigma_1 + \frac{\delta\mu}{|A|^2}\left[U + \frac{1 + C_3\mu^2 + C_4\mu^4 - \mu^2\omega^2(1 + C_1\mu^2)}{2\omega(1 + C_3\mu^2 + C_4\mu^4)}gb\right]. \tag{67}$$

The resulting solution is

$$A = a_0 \mathrm{e}^{-\mathrm{i}(\omega_2 a_0^2 T_2)}, \tag{68}$$

where $a_0 = |A|$. The leading-order solution for η is then

$$\eta_1 = a_0 \cos(kx - \tilde{\omega}t), \tag{69}$$

where

$$\tilde{\omega} = \omega + (\delta\mu)^2\omega_2 a_0^2. \tag{70}$$

Figure 11 shows a comparison of the ratio σ_1 from the present model and from the WKGS model to the Stokes' solution to the full problem. Figure 12 shows a similar comparison for σ_2. For both quantities, the present model exhibits better asymptotic behaviour for small μ-values. However, predictions begin to deviate from the full theory for values of μ as low as 0.5, and, for large μ-values, results of the higher-order ($O(\mu^4)$) theory deviate more rapidly from the full theory. Errors in the $O(\mu^4)$ model coefficients are on the order of 20% in the range $0 < \mu < 3$.

For the case of modulated wave trains, it has been shown (see Mei 1989) that the Stokes wave train is unstable to long-wavelength modulations in situations where ω'' and $\sigma = \sigma_1 + \sigma_2$ have different signs. For the full intermediate depth theory, it is well known that the boundary between stability and instability occurs at $\mu = 1.36$. This boundary corresponds to a change in sign of σ from positive in deep water to negative in shallow water, with $\omega'' < 0$ everywhere. For the present theories, the expressions for ω'' have sign changes at large values of μ, with the change occurring near $\mu = 3.8$ in the WKGS equations but far into the deep-water range for the present theory, as shown in figure 9. These sign changes would indicate a false restabilization of deep-water wave trains for the model equations being considered.

https://doi.org/10.1017/S0022112099007247 Published online by Cambridge University Press

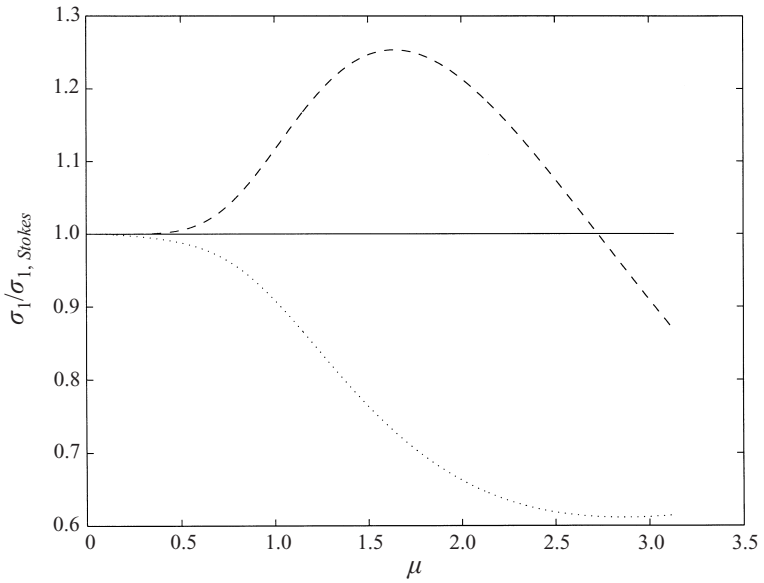


FIGURE 11. Ratio of Schrödinger equation cubic term coefficient σ_1 for the approximate models to the full problem solution. Wave–wave interaction contribution. WKGS (dot), present (dash).

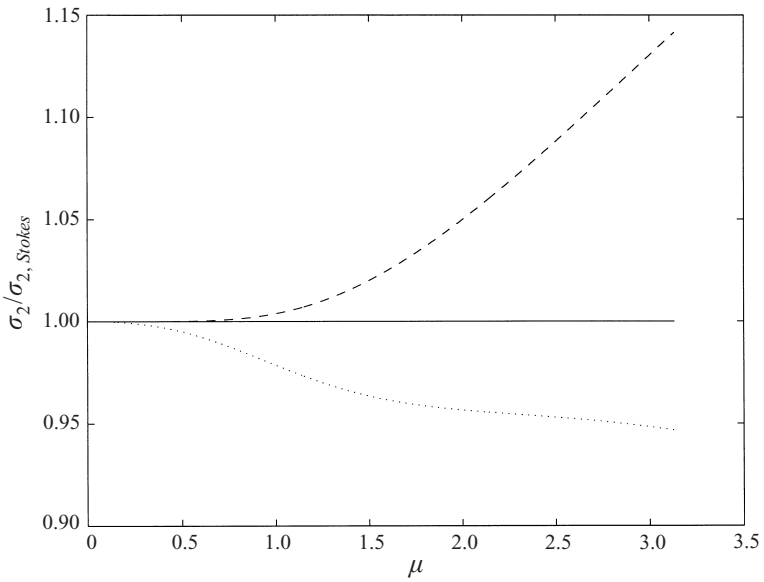


FIGURE 12. Ratio of Schrödinger equation's cubic term coefficient σ_2 for the approximate models to the full problem solution. Wave–current interaction contribution. WKGS (dot), present (dash).

Closer to shore, the present model's prediction of σ (figure 10) shows a shift in the zero-crossing of σ towards a somewhat shallower value close to $\mu = 1.2$, whereas the WKGS model results correspond to a shift to a somewhat deeper value near $\mu = 1.67$. This deviation would allow (for the $O(\mu^4)$ theory) envelope instabilities to persist into somewhat shallower depths than would be expected in the full theory.

https://doi.org/10.1017/S0022112099007247 Published online by Cambridge University Press

The magnitude of the deviation from the full theory is about the same for each order of the approximation.

5. Solitary waves

The phenomenon known as the solitary wave consists of a limiting wave form with a single crest which propagates in fairly shallow water of constant depth, and where the nonlinear and dispersive effects counterbalance each other yielding a permanent-form solution. In this section we study solitary waves solutions of the present fully nonlinear $O(\mu^4)$ FN4 model, and compare it to other models including extremely accurate solutions of the full boundary value problem (Tanaka 1986), Green & Naghdi (1976) (GN)-type models given by Shields & Webster (1988), and the WKGS model.

Many authors have found approximate solutions for the solitary wave, including the early works of Boussinesq (1871) and Korteweg & de Vries (1895). Fenton (1972) developed a model based on a perturbation expansion around the basic shallow water wave theory. His expansion includes terms up ninth order and, at the first three orders, recovers the models of Boussinesq (1871), Laitone (1960), and Grimshaw (1971). Longuet-Higgins & Fenton (1974) used conservation of integral quantities such as mass and energy to arrive at extremely accurate relationships between several solitary wave properties, such as the wave height, energy, mass, wave Froude number F_r (non-dimensional wave speed), etc. They also proved that the solitary wave with maximum wave height does not correspond to the one with maximum fluid velocity at the crest, or maximum mass. More recently, in a study of the stability of solitary waves, Tanaka (1986) developed an accurate solution scheme for the full boundary value problem for solitary waves. Throughout this section we will use this solution as the 'exact' solution in our comparisons. Shields & Webster (1988) studied the accuracy of solitary wave properties of the first three levels of a Green–Naghdi-like model, referred to hereafter as GN1, GN2, and GN3. An nth-level GN model approximates the horizontal velocity by an $(n-1)$th polynomial, and the vertical velocity by an nth-order polynomial, and is thus fundamentally rotational. GN1 recovers the model by Serre (1953), as shown by Kirby (1997). Shields & Webster (1988) derived a GN2 set of equations for unsteady flow over an uneven bottom, and a GN3 model for one-dimensional steady flow over a flat bottom.

5.1. *Linear asymptotic solution*

At the tail of the solitary wave (away from the crest) the free-surface elevation η is very small, and we expect that the linearized set of equations should describe the shape of the wave with good accuracy. In a reference frame moving with the wave at non-dimensional wave speed $F_r = c/\sqrt{gh}$, we can write the following boundary value problem for the wave field far from the crest (located at $x = 0$) in (x, z):

$$\nabla^2 \phi = 0, \tag{71}$$

$$\phi_x = -F_r, \qquad x \to \infty, \tag{72}$$

$$\phi_z = 0, \qquad z = -1, \tag{73}$$

$$\phi_z = -F_r^2 \phi_{xx}, \qquad z = 0. \tag{74}$$

The solution to the system above is

$$\phi = K_1 \mathrm{e}^{2\gamma x} \cos 2\gamma(1+z) - F_r x. \tag{75}$$

https://doi.org/10.1017/S0022112099007247 Published online by Cambridge University Press

Substituting (75) into (74) gives

$$\frac{\tan 2\gamma}{2\gamma} = F_r^2. \tag{76}$$

The exact solution for the free-surface elevation η far from the crest is of the form

$$\eta = K_2 \mathrm{e}^{2\gamma x}. \tag{77}$$

The parameter γ is referred to as the straining parameter, and (76) is directly related to the exact dispersion relationship in linear wave theory.

For the present model, the two equations corresponding to the system (71)–(74), in terms of the modified velocity variable $\tilde{u}$ are

$$\eta = F_r(\tilde{u} - C_3\tilde{u}_{xx} + C_4\tilde{u}_{xxxx}), \tag{78}$$

$$F_r\eta = (\tilde{u} - C_1\tilde{u}_{xx} + C_2\tilde{u}_{xxxx}), \tag{79}$$

where C_1, C_2, C_3, C_4 are defined in (20)–(23). We now assume the solution

$$\tilde{u} = \mathrm{e}^{2\gamma x}. \tag{80}$$

Substituting (80) into (78), (79), solving for $4\gamma^2$ and keeping the relevant root, we obtain

$$4\gamma^2 = \frac{(C_3F_r{}^2 - C_1) - \left[(C_3F_r{}^2 - C_1)^2 + 4(1 - F_r{}^2)(C_4F_r{}^2 - C_2)\right]^{1/2}}{2(C_4F_r{}^2 - C_1)}. \tag{81}$$

The expressions for the relation between the straining parameter and the Froude number for GN2 and GN3 (Shields 1986 and Shields & Webster 1988) are

$$2\gamma^2 = \tfrac{1}{3}(52 - 12F_r^{-2} - 4\sqrt{9F_r^{-4} - 33F_r^{-2} + 124}), \tag{82}$$

and

$$16F_r^2\gamma^6 + 60(1 - 9F_r^2)\gamma^4 - 20(39 - 144F_r^2)\gamma^2 + 1575(1 - F_r^2) = 0, \tag{83}$$

respectively.

Figure 13 shows a comparison of the percentage error to the exact solution of the transcendental equation (76) for γ, between the present model, Nwogu's model, GN2, and GN3. Although all models have relatively small errors, the present model is much more accurate than all the others by at least an order of magnitude. Notice that compared to GN2 and Nwogu's model, the difference in the errors is of at least five orders of magnitude.

5.2. *Numerical properties of solitary waves*

In this subsection, an extension of the numerical scheme of WKGS is used to compute several approximate solitary wave solutions to the fully nonlinear models FN4 and WKGS. Details of the numerical scheme may be found in Gobbi & Kirby (1999) or Gobbi (1998). The initial condition used for the model was constructed from the computer program by Tanaka (1986) in the following manner: for the smallest computed wave with amplitude $\eta_{max} \approx 0.2$, η and $\tilde{u}$ (u_α in the case of WKGS) were obtained from Tanaka's exact solution and used as initial condition for FN4 and WKGS. After the solution reached permanent form, it was multiplied by a factor slightly larger than 1 (typically 1.05) and this re-scaled wave was used as the initial condition for the next case. This procedure was repeated until the desired range of solitary waves was covered, and proved to be more efficient than using Tanaka's

https://doi.org/10.1017/S0022112099007247 Published online by Cambridge University Press

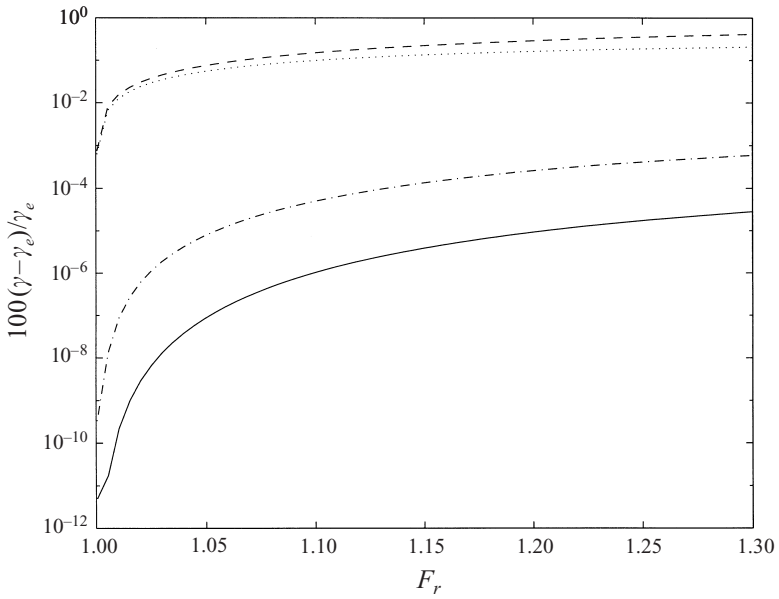


FIGURE 13. Percentage error to exact solution in straining parameter. Present model (full), Nwogu (dash), GN2 (dot), GN3 (dash–dot).

solution as the initial condition for all amplitudes. Since Tanaka's and each consecutive re-scaled initial condition do not satisfy the approximate equations, there is a transient period while the solution is not a permanent-form solitary wave, but has a dispersive tail of shorter waves left behind. Since these shorter waves travel with phase speeds which are smaller than the 'main wave', eventually the tail is left far behind and does not interfere with the solitary wave, which, at this point, can propagate with permanent form. The time required for the solution to achieve a permanent-form solitary wave depends on the initial condition. High-amplitude initial conditions will reach permanent form more quickly, since the primary wave moves much faster than the tail. Smaller-amplitude waves will have less amplitude dispersion and it will take longer for the permanent-form solitary wave to separate from the tail. After each solution reaches permanent form it is straightforward to obtain properties such as the Froude number, velocity profiles, mass, energy, etc. No filtering was necessary during these computations, although for higher waves the under-relaxation parameter had to be as small as $r = 0.08$ for the solution to converge with error tolerance in the iteration typically $10^{-12} \leqslant T_{err} \leqslant 10^{-9}$. For the permanent-form solitary waves we used grid spacing $\Delta x = 0.1h$ for waves with amplitude $0 < \eta_{max} < 0.4h$, $\Delta x = 0.05h$ for $0.4h < \eta_{max} < 0.7h$, and $\Delta x = 0.025h$ for $\eta_{max} > 0.7h$, where $h = 1$. We used Δt such that the Courant number was always below 0.2 (for accuracy purposes).

We now present the following non-dimensional quantities for the FN4 model, where the scales for the basic variables are $x = x'h$, $z = z'h$, $t = t'/\sqrt{g/h}$, $u = u'\sqrt{gh}$, and the primes denote non-dimensional quantities. The primes in the formulas below are dropped for the sake of notational clarity. The total mass of the solitary wave above the still water level is given by

$$M = \int_{-\infty}^{+\infty} \eta \, \mathrm{d}x. \tag{84}$$

https://doi.org/10.1017/S0022112099007247 Published online by Cambridge University Press

The potential energy is

$$V = \int_{-\infty}^{+\infty} \tfrac{1}{2}\eta^2 \,\mathrm{d}x. \tag{85}$$

The kinetic energy is

$$K = \frac{1}{2}\int_{-\infty}^{+\infty}\int_{0}^{H} (u^2 + w^2)\,\mathrm{d}\zeta\,\mathrm{d}x, \tag{86}$$

where $\zeta = (1+z)$, $H = 1 + \delta\eta$,

$$u(\zeta) = \tilde{u} + \tfrac{1}{2}\mu^2(B - \zeta^2)\tilde{u}_{xx} + \tfrac{1}{4}\mu^4(B^2 - B\zeta^2 - \tfrac{1}{6}D + \tfrac{1}{6}\zeta^4)\tilde{u}_{xxxx}, \tag{87}$$

and

$$w(\zeta) = \mu^2\zeta\tilde{u}_x + \mu^4[(\tfrac{1}{2}B\zeta + \tfrac{1}{6}\zeta^3)\tilde{u}_{xxx}]. \tag{88}$$

After substitution of (87) and (88) into (86) and retaining terms of up to $O(\mu^4)$, we obtain

$$\begin{aligned} K = \frac{1}{2}\int_{-\infty}^{+\infty} H\big\{&\big[\tilde{u}^2 + \mu^2(B - \tfrac{1}{3}H^2)\tilde{u}\tilde{u}_{xx}\big] \\ &+\tfrac{1}{2}\mu^4\left[(B - \tfrac{1}{3}H^2)B - \tfrac{1}{6}(D - \tfrac{1}{5}H^4)\right]\tilde{u}\tilde{u}_{xxxx} \\ &+\tfrac{1}{4}\mu^4(B^2 - 2B\tfrac{1}{3}H^2 + \tfrac{1}{5}H^4)\tilde{u}_{xx}^2 + \tfrac{1}{3}\mu^4H^2\tilde{u}_x^2\big\}\,\mathrm{d}x. \end{aligned} \tag{89}$$

The integrals in x are computed using Bode's rule, which is accurate to $O(\Delta x^6)$.

We define the quantity

$$\omega_s = 1 - (u_c - F_r)^2, \tag{90}$$

where u_c is the particle velocity at the crest, computed from (87) by locating the position of the crest in x and computing $u(\zeta = H)$ at that x location. As the wave amplitude varies from 0 to its limiting value, in which $u_c = F_r$, the parameter ω_s goes from 0 to 1.

The speed of each wave was computed by letting an already permanent-form solution propagate over a distance of around 500 times the water depth, recording the difference between the crest location x_c before and after this interval $\mathrm{d}t$ and computing

$$F_r = \frac{\mathrm{d}x_c}{\mathrm{d}t}. \tag{91}$$

The exact location of the wave crest could not be obtained directly from the computations, since only by virtue of luck was the crest located exactly at one of the grid points. The location of the crest was determined by fitting a fourth-order polynomial to the free surface around the crest. The peak value and x location were then computed using the fitted polynomial. We used this same approach to compute $\tilde{u}$ and its x-derivatives at and underneath the crest.

Figure 14 shows computations of the free-surface elevation of half of a solitary wave with $F_r = 1.266$ for FN4, WKGS, GN1, GN2, GN3, and the exact solution. The three GN models are plotted with dotted lines, with GN1 and GN2 marked with labels. Notice that, of all models, GN3 has the best match with the exact solution. FN4 is also fairly close to the exact solution, but WKGS strongly overpredicts the wave height, and slightly underpredicts the tail. GN models tend to underpredict the height and overpredict the tail. Figure 15 shows the same model comparisons as in figure 14, except for GN1 and GN2 whose solutions were not available. In this case the

https://doi.org/10.1017/S0022112099007247 Published online by Cambridge University Press

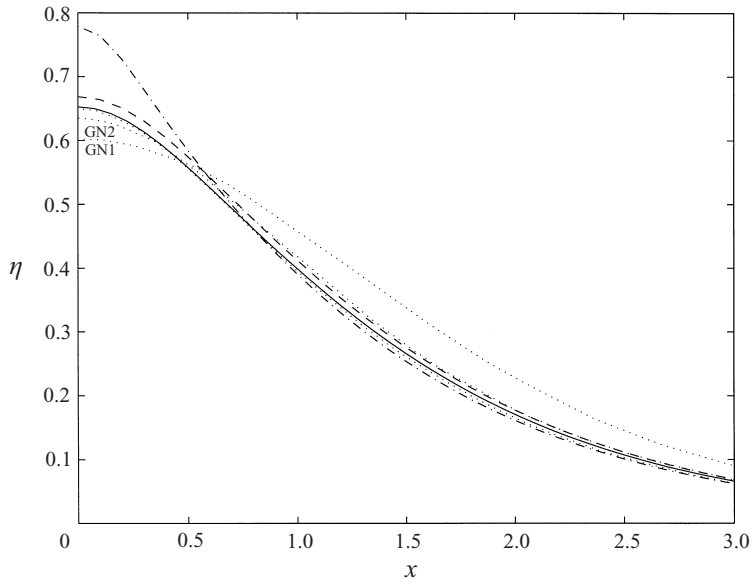


FIGURE 14. Shape of solitary waves with fixed $F_r = 1.266$. Exact (full), FN4 (dash), WKGS (dash–dot), GN1, GN2, GN3 (dot).

maximum wave height is kept constant for all models. Again, GN3 has the best shape compared to the exact solution. The WKGS solution compares better with the exact solution than in the previous case (F_r kept constant), but FN4 still compares better with the exact solution than does WKGS. Notice also the difference in wave speed F_r for each model. In figure 16 the vertical profiles of the horizontal velocity are shown for the exact solution, FN4, and WKGS, for the waves shown in figure 14, and it can be seen that the $O(\mu^4)$ model has a more accurate kinematic representation than the $O(\mu^2)$ model, confirming what we have already shown for linear theory. Unfortunately it was not possible to obtain GN vertical profiles, but it can be speculated that that model would not be able to predict this property as accurately as the FN4, since it assumes the horizontal velocity to be only a second-order polynomial.

Figure 17 shows the relationship between the speed and amplitude of a wide range of solitary waves for several models. Notice that once again GN3 has the closest solution to the exact one. FN4 slightly underpredicts the wave speed for a given amplitude, whereas the deviation in WKGS is of an order of magnitude higher. GN2 and especially GN1 overpredict the wave speed throughout the range tested. It is important to keep in mind that as the wave approaches the limiting value, the crest becomes extremely sharp (with the limiting wave having a crest forming an angle of 120°), which makes it difficult for the finite difference scheme of FN4 to resolve the wave well near the crest, since the model has up to fifth-order derivatives in x.

Figure 18 shows computations of the parameter ω_s as a function of the wave speed. In this case, the FN4 model is the closest to the exact solution. This is not surprising if one recalls that ω_s is directly related to the horizontal fluid velocity at the crest, and that FN4 has a fourth-order polynomial representation of the vertical profile of the horizontal velocity, whereas, as already observed, only a second-order polynomial is assumed in both GN3 and WKGS. In the next figures, GN solutions were not available. Figures 19, 20, and 21 show plots of the mass, kinetic energy, and potential energy of solitary waves against the wave speed, for the exact solution, FN4,

https://doi.org/10.1017/S0022112099007247 Published online by Cambridge University Press

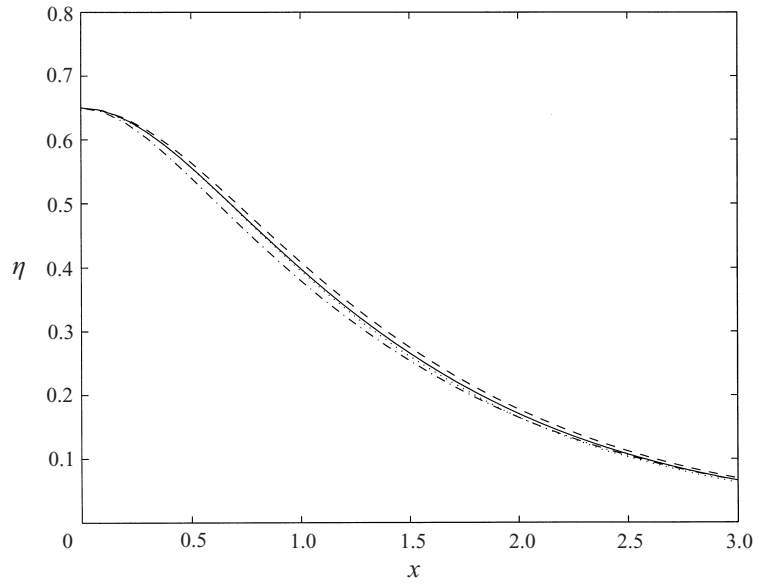


FIGURE 15. Shape of solitary waves with fixed amplitude $\eta_{max} = 0.65$. Exact: $F_r = 1.265$ (full), FN4: $F_r = 1.262$ (dash), WKGS: $F_r = 1.245$ (dash–dot), GN3: $F_r = 1.266$ (dot).

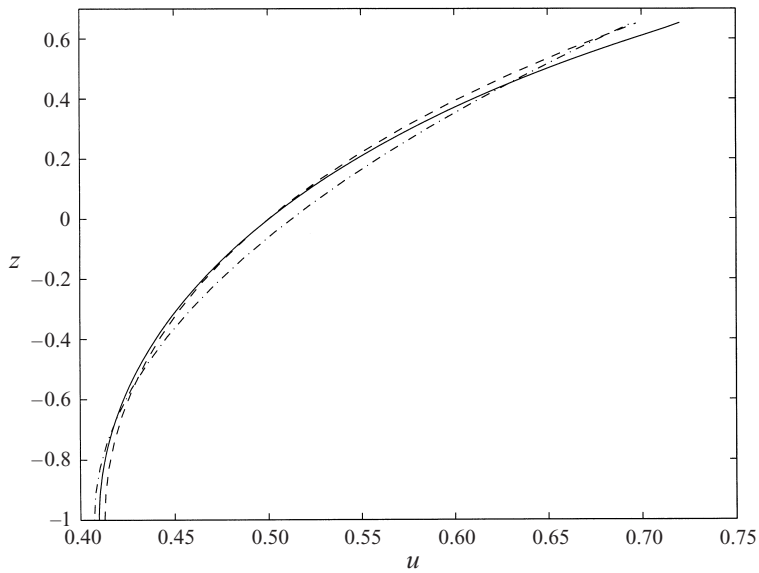


FIGURE 16. Vertical profile of horizontal velocity for solitary waves with amplitude $\eta_{max} = 0.65$. Exact (full), FN4 (dash), WKGS (dash–dot).

and WKGS. All three properties show a similar behaviour to the wave amplitude (figure 17) when plotted against F_r. In figure 19, WKGS agrees with the exact solution better than FN4, but this is only a coincidence, as the overprediction of the wave crest counterbalances the underprediction of the wave tail. A similar effect happens with the kinetic energy (figure 20), where the plots of the two models coincidently are on top of each other. The potential energy (figure 21) calculations for model

https://doi.org/10.1017/S0022112099007247 Published online by Cambridge University Press

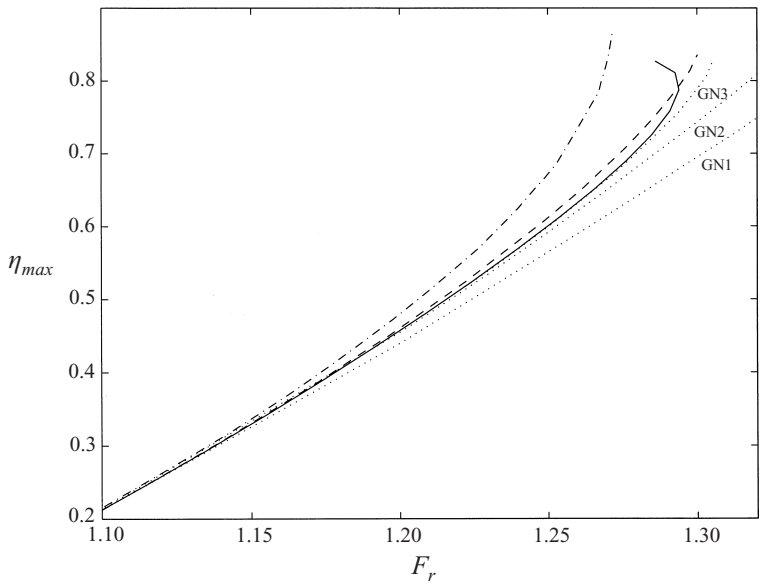


FIGURE 17. Solitary wave amplitude vs. phase speed. Exact (full), FN4 (dash), WKGS (dash–dot), GN1, GN2, GN3 (dot).

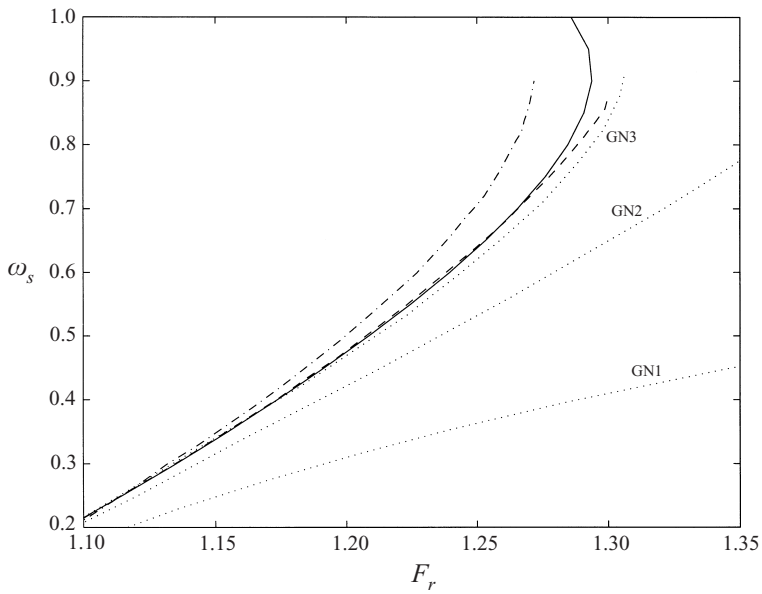


FIGURE 18. ω_s vs. phase speed for solitary waves. Exact (full), FN4 (dash), WKGS (dash–dot), GN1, GN2, GN3 (dot).

FN4 has better agreement with the exact solution than it has with the WKGS model, which confirms that the good agreement of WKGS in figure 17 was by virtue of luck, since both the mass and the potential energy are only dependent on the free-surface elevation.

https://doi.org/10.1017/S0022112099007247 Published online by Cambridge University Press

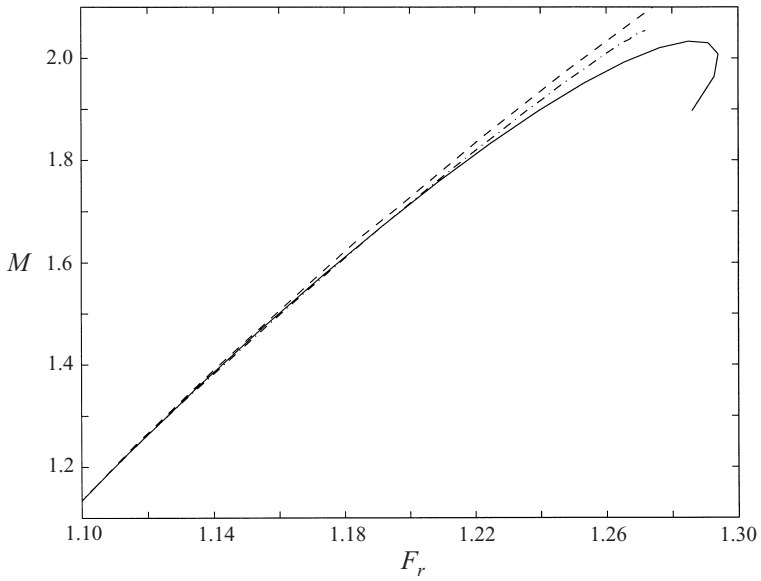


FIGURE 19. Mass vs. phase speed for solitary waves.
Exact (full), FN4 (dash), WKGS (dash–dot).

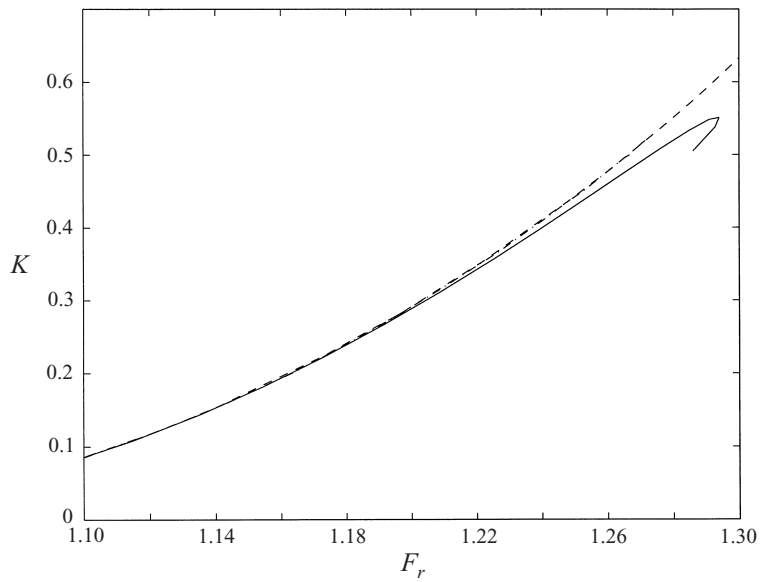


FIGURE 20. Kinetic energy vs. phase speed for solitary waves.
Exact (full), FN4 (dash), WKGS (dash–dot).

5.3. *Discussion*

From figures 13, 14, 15, 17, 18, it is clear that the FN4 model has a better asymptotic (linear) agreement with the exact solution than does GN3, but, with the exception of the parameter ω_s (related to the velocity at the crest of the wave), in all other nonlinear properties, GN3 has a better agreement than FN4. This may seem somewhat surprising since GN3 approximates the horizontal velocity by a second-order

https://doi.org/10.1017/S0022112099007247 Published online by Cambridge University Press

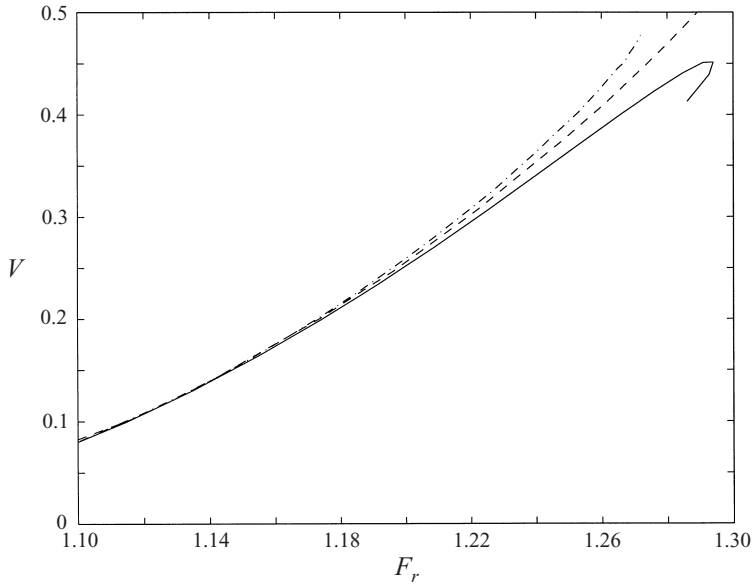


FIGURE 21. Potential energy vs. phase speed for solitary waves. Exact (full), FN4 (dash), WKGS (dash–dot).

polynomial (two orders lower than the FN4 model) and the vertical velocity by a third-order polynomial (same as the FN4 model), and a more careful study is needed to explain these discrepancies. Nevertheless, we make the following conjectures: FN4 satisfies mass conservation and all boundary conditions in an approximate sense, consistent with the level of approximation of the velocity field. GN3 satisfies mass conservation and the kinematic boundary conditions exactly. The coefficients for the velocity variable in FN4 are derived such that the linear dispersion relationship is extremely accurate, and no optimization is done considering that the free-surface displacement is finite or including nonlinear terms. The advantage of this approach is that the model is simple in the sense that there is only one dependent variable describing the internal kinematics. For small-amplitude waves the FN4 model is capable of extremely accurate results for a wide range of water depths, but as the nonlinear terms become more important, and the actual free surface deviates considerably from the still water level (for which the model was derived to perform its best), errors start to increase. On the other hand, GN3 is derived without any *a priori* assumption about the relation between the values of model coefficients for each term in the vertical polynomial representation. Rather, the coefficients for the velocity polynomial are obtained through a minimization of the errors in the momentum equation over the entire actual water depth, which is changing with time. As a consequence, GN3 has three dependent variables describing each component of the velocity field, besides the free-surface elevation. For a two-dimensional problem, GN3 would have seven coupled evolution equations, whereas FN4 would have three. The present model is thus simpler in structure than the GN3 approximation and has been successfully implemented for the time-dependent case of irregular wave trains.

https://doi.org/10.1017/S0022112099007247 Published online by Cambridge University Press

6. Conclusions

A Boussinesq-type model with $O(1)$ nonlinearity and $O(\mu^4)$ dispersion has been proposed. By defining one of the dependent variables as the weighted average of the velocity potential at two distinct water depths, it is possible to achieve an accurate (4,4) Padé approximant for the linear dispersion relationship. A major improvement over the existing second-order models has been found in the prediction of the linear internal flow kinematics. A perturbation approach was carried out to analyse random wave second-order nonlinear interactions and it has been shown that the present model predicts very well the transfer coefficients of super- and subharmonic generation over a wide range of water depths. A cubic nonlinear Schrödinger equation governing the propagation of the wave envelope was obtained by a standard WKB perturbation multiple scales approach and its coefficients were compared to those of the full model as well as of the WKGS $O(\mu^2)$ model. The present model's cubic term coefficient deviates from the prediction of the full Stokes theory, moving the transition from unstable behaviour in intermediate depth to stable behaviour in shallow water to a kh value of 1.2. The result of errors of this type on the shoreward evolution of wave groups in intermediate water depths has not been extensively explored in the literature on Boussinesq equations, and would be a worthy topic for further investigation.

Properties of solitary waves were obtained numerically and were compared to exact results and the first three levels of approximation in the theory of Shields & Webster (1988). The resulting FN4 model is found to have comparable accuracy to the GN3 or third level of approximation except for a slight underprediction of phase speeds for high-amplitude solitary waves.

Algorithms for the numerical solution of the present FN4 model are described in Gobbi & Kirby (1999), where the model is applied to the study of wave shoaling and harmonic generation in the problem of waves propagating over an isolated step. Results for this case have been further compared to results from the local polynomial approximation method of Kennedy & Fenton (1997) in Gobbi, Kennedy & Kirby (1998).

This work was supported by the Army Research Office through University Research Initiative Grant DAAL 03-92-G-0116, and by the Brazilian agency Fundação Capes.

Appendix A. Application of Nwogu's (1993) method at $O(\mu^4)$

The procedure of Nwogu (1993) rests on choosing the potential or velocity at an elevation z_α in the water column such that the resulting linear dispersion relationship of the model is optimal in some sense. As pointed out by Dingemans (1997), this procedure does not produce the desired (4,4) Padé level of approximation discussed in the text. The dispersion relationship in a model retaining terms to $O(\mu^2)$ is given by

$$\omega^2 = \frac{1-(\alpha+\frac{1}{3})\mu^2}{1-\alpha\mu^2}, \tag{A 1}$$

where

$$\alpha = \tfrac{1}{2}z_\alpha^2 + z_\alpha. \tag{A 2}$$

The choice $\alpha = -\frac{2}{5}$ reproduces the (2,2) Padé approximant, while the choice $\alpha = -0.39$ proposed by Nwogu minimizes the error (in a least-square sense) in the dispersion relation over the range $0 \leqslant \mu \leqslant \pi$.

https://doi.org/10.1017/S0022112099007247 Published online by Cambridge University Press

Following Nwogu's procedure, we extend the approximate expression for the velocity potential (in terms of ϕ_α) to $O(\mu^4)$ and obtain

$$\phi = \phi_\alpha + \tfrac{1}{2}\mu^2\left[(1+z_\alpha)^2-(1+z)^2\right]\nabla^2\phi_\alpha + \tfrac{1}{24}\mu^4\left[5(1+z_\alpha)^4-6(1+z_\alpha)^2(1+z)^2+(1+z)^4\right]\nabla^2\nabla^2\phi_\alpha + O(\mu^6). \quad \text{(A 3)}$$

This expression is used in linearized versions of (5) and (3) to obtain the linear model

$$\eta_t + \nabla^2\phi_\alpha + \mu^2(\alpha+\tfrac{1}{3})\nabla^2\nabla^2\phi_\alpha + \mu^4(5\alpha^2+4\alpha+\tfrac{4}{5})\nabla^2\nabla^2\nabla^2\phi_\alpha = 0, \quad \text{(A 4)}$$

$$\eta + \phi_{\alpha t} + \mu^2\alpha\nabla^2\phi_{\alpha t} + \mu\tfrac{1}{6}\alpha(2+5\alpha)\nabla^2\nabla^2\phi_{\alpha t} = 0. \quad \text{(A 5)}$$

The corresponding linearized dispersion relation is given by

$$\omega^2 = \frac{1-(\alpha+\frac{1}{3})\mu^2+(5\alpha^2+4\alpha+\frac{4}{5})\alpha^4}{1-\alpha\mu^2+(\frac{5}{6}\alpha^2+\alpha/3)\mu^4}. \quad \text{(A 6)}$$

This is equivalent to Nwogu's result if terms of $O(\mu^4)$ are dropped. The resulting dispersion relation contains only a single parameter, and there is no choice of α which reproduces the desired (4,4) Padé approximant. Dingemans (1997) shows results for the choice $\alpha = -\frac{4}{9}$, which corresponds to reproducing the coefficients of the $O(\mu^2)$ terms in (7).

Appendix B. Expressions appearing in § 4 equations

$$\sigma_1 = \frac{-P_{22}}{\omega Q_1 Q_2}\left[4+16C_1\mu^2-\omega^{-2}(1+4C_3\mu^2+16C_4\mu^4)\right] - \frac{\omega}{2Q_1}(E_{20}+E_{22})(\mu+C_1\mu^3-\omega^{-2}\mu^{-1}Q_1) + \frac{P_{22}}{4\mu^2\omega^3Q_1^2Q_2}\left[1+(2+5C_3)\mu^2+(10C_1+17C_4+4C_3^2)\mu^4\right] - \frac{3}{16Q_1}\left[1+C_3\mu^2-\omega^{-2}(1+C_1\mu^2)\right]+\frac{1}{\omega Q_1^2}\left[4+(8C_3+1/6)\mu^2\right], \quad \text{(B 1)}$$

$$\sigma_2 = \frac{\left((1/2\omega\mu^2)-C_gQ_3\right)}{2(C_g^2-1)}\left[\frac{C_g}{\omega Q_1}\left\{Q_1-\mu^2(1+C_1\mu^2)\right\}+\left(1+\frac{1}{Q_1}\right)\right], \quad \text{(B 2)}$$

where

$$Q_1 = 1+C_3\mu^2+C_4\mu^4, \quad \text{(B 3)}$$

$$Q_2 = 4(1+\omega^{-2})(1+4C_1\mu^2+4C_4\mu^4), \quad \text{(B 4)}$$

$$Q_3 = \frac{1}{2Q_1}\{1-C_1\mu^2\}+\frac{1}{4\omega^2Q_1^2\mu^2}\{1+(2C_3+1)\mu^2+(2C_4+C_3^2+2C_1)\mu^4\}, \quad \text{(B 5)}$$

$$P_{22} = -2\left[Q_1-\mu^2(1+C_1\mu^2)\right]-Q_1^{-1}\left[2Q_1-1-\mu^2-(2C_1-C_3^2)\mu^4\right], \quad \text{(B 6)}$$

$$E_{20} = \frac{\mu}{2Q_1}(1+C_1\mu^2)-\frac{1}{\mu\omega^2Q_1^2}\left[2Q_1-1+\mu^2+(2C_1+C_3^2)\mu^4\right], \quad \text{(B 7)}$$

https://doi.org/10.1017/S0022112099007247 Published online by Cambridge University Press

$$E_{22} = \frac{1}{2\omega^2 Q_2 Q_1} P_{22}(1 + 4C_3\mu^2 + 16C_4\mu^4)$$

$$+\frac{\mu}{4Q_1}(1 + C_1\mu^2) - \frac{1}{\mu\omega^2 Q_1^2}\left[2Q_1 - 1 - \mu^2 + (2C_1 - C_3^2)\mu^4\right], \qquad \text{(B 8)}$$

C_1–C_4 are given in (20)–(23). The corresponding σ_1 and σ_2 for the full boundary value problem are given by

$$\sigma_1 = \frac{\cosh 4\mu + 8 - 2\tanh^2\mu}{16\sinh^4\mu}, \qquad \text{(B 9)}$$

$$\sigma_2 = \frac{1}{2\omega(C_g^2 - 1)}\left(1 + \frac{C_g}{2\omega\cosh^2\mu}\right)^2. \qquad \text{(B 10)}$$

REFERENCES

Boussinesq, J. 1871 Theorie de l'intumescence liquide appelee onde solitaire ou de translation se propageant dans un canal retangulaire. *C. R. Acad Sci. Paris* **72**, 755–759.

Chen, Q. R., Dalrymple, A., Kirby, T., Kennedy, A. & Haller, M. C. 1999 Boussinesq modelling of a rip current system. *J. Geophys. Res.* **104**, 20617–20637.

Chen, Y. & Liu, P. L.-F. 1995 Modified Boussinesq equations and associated parabolic models for water wave propagation. *J. Fluid Mech.* **288**, 351–381.

Dingemans, M. 1973 Water wave over uneven bottom; a discussion of long wave equations. *Rep.* R729, part 2. Delft Hydraulics.

Dingemans, M. 1997 *Water Wave Propagation over Uneven Bottoms*. World Scientific.

Fenton, J. D. 1972 A ninth-order solution for the solitary wave. *J. Fluid Mech.* **53**, 237–246.

Gobbi, M. F. 1998 A new Boussinesq-type model for surface water wave propagation. Dissertation, University of Delaware.

Gobbi, M. F., Kennedy, A. B. & Kirby, J. T. 1998 A comparison of higher-order Boussinesq and local polynomial approximation models. *Proc. 26th Intl Conf. Coastal Engng* (ed. B. Edge), pp. 631–644. ASCE.

Gobbi, M. F. & Kirby, J. T. 1999 Wave evolution over submerged sills: Tests of a high-order Boussinesq model. *Coast. Engng* **37**, 57–96.

Green, A. E. & Naghdi, P. M. 1976 A derivation of equations for wave propagation in water of variable depth. *J. Fluid Mech.* **78**, 237–246.

Grimshaw, R. 1971 The solitary wave in water of variable depth. *J. Fluid Mech.* **86**, 415–431.

Hasselmann, K. 1962 On the nonlinear energy transfer in a gravity wave spectrum. *J. Fluid Mech.* **12**, 481–500.

Kennedy, A. B. & Fenton, J. D. 1997 A fully-nonlinear computational method for wave propagation over topography. *Coast. Engng* **32**, 137–161.

Kirby, J. T. 1997 Gravity waves on water of variable depth. In *Advances in Fluid Mechanics, 10* (ed. J. N. Hunt), pp. 55–125. Computational Mechanics Publications.

Kirby, J. T. & Wei, G. 1994 Derivation and properties of a fully nonlinear, extended Boussinesq model. In *Proc. IAHR Symposium: Waves – Physical and Numerical Modelling*, pp. 386–395.

Korteweg, D. J. & Vries, G. de 1895 On the change of form of long waves advancing in a rectangular canal and on a new type of long stationary wave. *Phil. Mag.* (5) **39**, 422–443.

Laitone, E. V. 1960 The second approximation to cnoidal and solitary waves. *J. Fluid Mech.* **9**, 430–444.

Longuet-Higgins, M. S. & Fenton, J. D. 1974 On the mass, momentum, energy and circulation of a solitary wave. *Proc. R. Soc. Lond.* A **340**, 471–493.

Madsen, P. A., Banijamali, B., Schäffer, H. A. & Sørensen, O. R. 1996 Boussinesq type equations with high accuracy in dispersion and nonlinearity. *Proc. 25th Intl Conf. Coastal Engng* (ed. B. Edge), vol. 1, pp. 95–108. ASCE.

Madsen, P. A., Murray, R. & Sørensen, O. R. 1991 A new form of Boussinesq equations with improved linear dispersion characteristics. *Coast. Engng* **15**, 371–388.

https://doi.org/10.1017/S0022112099007247 Published online by Cambridge University Press

Madsen, P. A. & Sørensen, O. R. 1992 A new form of Boussinesq equations with improved linear dispersion characteristics. Part 2. A slowly-varying bathymetry. *Coast. Engng* **18**, 183–204.

Madsen, P. A. & Sørensen, O. R. 1993 Bound waves and triad interactions in shallow water. *Ocean Engng* **20**, 359–388.

Madsen, P. A., Sørensen, O. R. &. Schäffer, H. A. 1997 Surf zone dynamics simulated by a Boussinesq type model. Part 1. Model description and cross-shore motion of regular waves. *Coast. Engng* **32**, 255–287.

Mei, C. C. 1989 *The Applied Dynamics of Ocean Surface Waves.* World Scientific.

Nwogu, O. 1993 An alternative form of the Boussinesq equations for nearshore wave propagation. *J. Waterway, Port, Coast., Ocean Engng* **119**, 618–638.

Peregrine, D. H. 1967 Long waves on a beach. *J. Fluid Mech.* **27**, 815–820.

Schäffer, H. A. & Madsen, P. A. 1995*a* Further enhancements of Boussinesq-type equations. *Coast. Engng* **26** (1–2), 1–15.

Schäffer, H. A. & Madsen, P. A. 1995*b* A new formulation of higher order Boussinesq equations. In *COASTAL 95, 6–8 September 1995, Cancun, Mexico*, pp. 159–166.

Schröter, A., Mayerle, R. & Zielke, W. 1994 Optimized dispersion characteristics of the Boussinesq wave equations. *Proc. Waves – Physical and Numerical Modelling*, pp. 416–425.

Serre, F. 1953 Contribution a l'etude des ecoulements permanents et variables dans les canaux. *La Houille Blanche* **3**, 374–388.

Shields, J. J. 1986 A direct theory for waves approaching a beach. Dissertation, University of California at Berkeley.

Shields, J. J. & Webster , W. C. 1988 On direct methods in water-wave theory. *J. Fluid Mech.* **197**, 171–199.

Tanaka, M. 1986 The stability of solitary waves. *Phys. Fluids* **29**, 650–655.

Wei, G., Kirby, J. T., Grilli, S. T. & Subramanya, R. 1995 A fully nonlinear Boussinesq model for surface waves. Part 1. Highly nonlinear unsteady waves. *J. Fluid Mech.* **294**, 71–92.

Witting, J. M. 1984 A unified model for the evolution of nonlinear water waves. *J. Comput. Phys.* **56**, 203–239.

https://doi.org/10.1017/S0022112099007247 Published online by Cambridge University Press